Scheduling and Power Control for V2V Broadcast Communications With Co-Channel and Adjacent Channel Interference

ANVER HISHAM[ID]1, ERIK G. STRÖM[ID]1, (Senior Member, IEEE),
FREDRIK BRÄNNSTRÖM1, (Member, IEEE), AND LI YAN2
[1]Department of Electrical Engineering, Chalmers University of Technology, 412 96 Gothenburg, Sweden
[2]Combitech AB, 417 56 Gothenburg, Sweden

Corresponding author: Anver Hisham (anver@chalmers.se)

ABSTRACT This paper investigates how to mitigate the impact of both the co-channel interference and the adjacent channel interference (ACI) in the vehicle-to-vehicle (V2V) broadcast communication by scheduling and power control. Our objective is to maximize the number of connected vehicles. The optimal joint scheduling and power control problem is formulated as a mixed integer programming problem with a linear objective and a quadratic constraint. From the joint formulation, we derive (a) the optimal scheduling problem for fixed transmit powers as a Boolean linear programming problem and (b) the optimal power control problem for a fixed schedule as a mixed integer linear programming problem. The near-optimal schedules and power values are computed by solving first (a) and then (b) for smaller-size instances of the problem. To handle larger-size instances of the problem, we propose heuristic scheduling and power control algorithms with less computational complexity. The simulation results indicate that the heuristic scheduling algorithm yields significant performance improvements compared to the baseline block-interleaver scheduler and that performance is further improved by the heuristic power control algorithm. Moreover, the heuristic algorithms perform close to the optimal scheme for small instances of the problem.

INDEX TERMS ACI, ACIR, SINR, scheduling, power control, optimization.

I. INTRODUCTION

A. MOTIVATION

Recently, vehicle-to-vehicle (V2V) communication have captured great attention due to its potential to improve traffic safety, effective driving assistance, and intelligent transport systems. The safety critical information, such as cooperative awareness messages (CAMs) and decentralized environmental notification messages (DENM) [1], requires spreading safety related messages among surrounding vehicles either in a periodic or event triggered way.

Conveying safety critical messages in V2V networks have different requirements compared to conventional cellular communication systems. First, disseminating safety critical messages generally rely on broadcast protocols and

often comes with a stringent requirement on reliability, which can be achieved if the signal to interference and noise ratio (SINR) exceeds a certain threshold [2]. Secondly, low latency is an important requirement which restricts the possibilities for retransmissions. Moreover, retransmissions are cumbersome in a broadcast communication scenario.

A key determining factor of reliability of a communication link is received interference power. There are two main types of interference: co-channel interference (CCI) and adjacent channel interference (ACI). The difference between these two lies in the frequency slot in which interferer transmits. CCI occurs when the interferer is transmitting on the same time-frequency slot as the intended transmitter. On the other hand, ACI occurs when the interferer is transmitting in the same timeslot, but on a nearby frequency slot.

The associate editor coordinating the review of this manuscript and approving it for publication was Mohammad S. Khan.
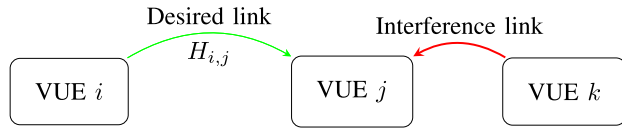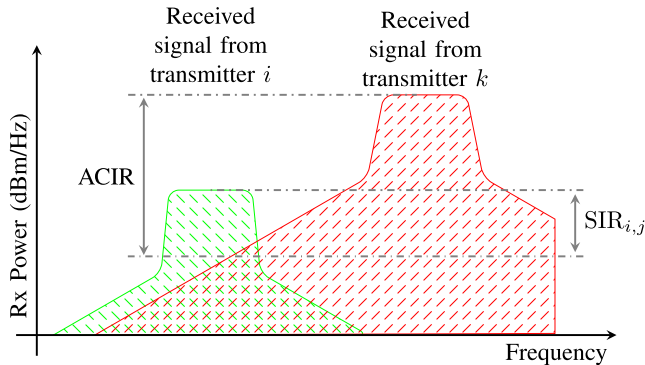
FIGURE 1. System model.

FIGURE 2. Received power spectral density at receiving VUE j.

ACI is mainly due to the nonlinearities in the power amplifier in the transmitter, which causes the transmitted spectrum to spread beyond what was intended. An example of ACI is illustrated in Fig. 1 and Fig. 2, where the receiver j is decoding signals from transmitter i. Although transmitter k is using a different frequency band, the signal to interference ratio $\mathrm{SIR}_{i,j}$ of receiver j while decoding the signal from transmitter i is limited by ACI from transmitter k.

ACI is typically not a problem in a cellular communication network, since interference is dominated by CCI due to the spectrum re-usage. Additionally, ACI is a significant problem in near-far situations only, i.e., when the interfering signal has much higher power than the desired one, see Fig. 2. In a cellular setting, ACI would be relative small in the uplink, if power control is used to equalize the received powers, and in the downlink, if the users associate with the closest base station (BS).

However, it is known that V2V channel power gains are quite dynamic: measurements indicate that blocking vehicles can introduce high penetration losses [3]–[6]. Hence, a transmitting vehicle need to use a high transmit power to reach a vehicle that is blocked by other vehicles, and this causes a near-far situation at vehicles that are not blocked. Moreover, unlike CCI, the received ACI is hard to cancel using interference cancellation techniques [7]. Therefore, ACI is a key factor in determining the performance in V2V communication, and ACI-unaware schedulers might be underperforming in the presence of ACI. Indeed, we see an example of a reasonable ACI-unaware scheduler in Section VII that is quite suboptimal when VUEs are multiplexed in frequency.

B. STATE OF THE ART
As pointed out above, ACI is typically not a problem in traditional cellular communication uplink/downlink

scenarios. Therefore, vast majority of the scheduling and power control literature ignore ACI and focuses upon reducing CCI alone [8]–[10]. However, in the absence of CCI, V2V broadcast communication performance is mainly limited by ACI [11]. In [12], the authors analyze the impact of ACI for device-to-device (D2D) communication, for various user densities and transmit powers, and conclude that ACI indeed causes outage problems when the user density is high. Similar conclusions have been made in [13], where the impact of ACI from cellular uplink to D2D communication is analyzed. In [14], authors experimentally assess the throughput degradation due to ACI in an OFDM based communication system 802.11a, and conclude that ACI impact is indeed significant. Similar studies have been done upon 802.11b/g/n/ac in [15]–[17]. The impact of ACI when different communication technologies coexist in adjacent frequency bands have been extensively studied in [18]–[21]. In [22], the authors assess the performance degradation due to ACI when two LTE base stations are deployed in adjacent frequency channels.

In V2V with carrier-sense multiple access (CSMA) medium access control (MAC), a potential transmitter may falsely assume that the channel is busy due to the ACI from a transmitter tuned to an adjacent channel, which causes the transmitter to defer its transmission resulting in delays [23], [24]. Additionally, in [24], the authors analyze both physical layer and MAC layer impacts of ACI in vehicular ad hoc networks (VANETs). Our previous work [11] studies the impact of ACI in V2V broadcast communication.

C. CONTRIBUTIONS
Our goal is to find scheduling and power control algorithms to maximize the number of connected vehicles in a V2V multicast communication scenario. The scheduling and power control is made by a centralized unit (e.g., a BS, roadside infrastructure node, or a special vehicle) based on slowly-varying channel state information (CSI), and communication between vehicles is direct (i.e, not via an uplink-downlink arrangement or via intermediate nodes). By this, we increase the mutual awareness of the state (position, speed, heading, etc.) of the connected VUEs, which in turn improves vehicular safety. We make following contributions to achieve this goal:

1) The impact of ACI in V2V broadcast communication is evaluated.
2) Joint scheduling and power control problem to maximize the connectivity is formulated as a mixed integer quadratically constrained programming (MIQCP) problem. From this joint problem, we derive a pure scheduling problem (for fixed transmit powers) as a Boolean linear programming (BLP) problem and a pure power control problem (for a fixed schedule) as a mixed integer linear programming MILP) problem. To the best of our knowledge, we are the first to formulate ACI-aware scheduling and power control problems. For

small instances of the joint problem, we compute a numerically optimal solution for scheduling by solving the BLP problem and then compute a numerically optimal power values by solving the MILP problem.

3) Due to the NP-hardness of the above scheduling problem, we suggest a block interleaver scheduler (BIS), which requires only the position indices of the VUEs.

4) We also propose a heuristic scheduling algorithm with polynomial time complexity. The simulation results show the promising performance of the proposed algorithm, compared to the BIS and optimal scheduler.

5) Due to the NP-hardness of the optimal power control problem, we propose a heuristic power control algorithm as an extension of our previous work in [11]. The simulation results show that the proposed algorithm further improves the performance compared to equal power.

D. NOTATION AND OUTLINE

We use the following notation throughout the paper. Sets are denoted by calligraphic letters, e.g., $\mathcal{X}$, with $|\mathcal{X}|$ denoting its cardinality, and $\emptyset$ indicate an empty set. Lowercase and uppercase letters, e.g., x and X, represent scalars. Lowercase boldface letters, e.g., $\mathbf{x}$, represent a vector where x_i is the ith element and $|\mathbf{x}|$ is its dimensionality. The uppercase boldface letters, e.g., $\mathbf{X}$, denote matrices where $X_{i,j}$ indicates the (i, j)th element. The notations $\lceil \cdot \rceil$, and $\lfloor \cdot \rfloor$, $\lfloor \cdot \rceil$ represents ceil, floor, and round operations, respectively.

The rest of the paper is organized as follows. We discuss system model and ACIR model in Section II. Section III formulates optimal scheduling and power control as an optimization problem. Sections IV and V describes scheduling algorithms and power control algorithms, respectively, with lower computational complexity than the optimum joint approach. The computational complexity and the overhead of the algorithms are analyzed in Section VI. Finally, we discuss numerical results in Section VII, draw conclusions in Section VIII, and describe future work in Section IX.

II. PRELIMINARIES

A. SYSTEM MODEL

The key mathematical symbols are summarized in Table 1. We consider a network of N VUEs, where the set of VUEs is denoted by $\mathcal{N} \triangleq \{1, 2, \ldots, N\}$. We indicate a transmitting VUE as VUE i, receiving VUE as VUE j, and interfering VUE as VUE k as illustrated in Fig. 1. The average channel power gain from VUE i to VUE j, which takes into account pathloss and large-scale fading, is denoted by $H_{i,j}$. We assume, without loss of generality, that VUE i wants to transmit its packet to all VUEs in the set $\mathcal{R}_i \subset \mathcal{N}$, and VUE j wants to receive packets from all VUEs in the set $\mathcal{T}_j = \{i : j \in \mathcal{R}_i\}$. Note that the unicast communication is the special case when $|\mathcal{R}_i| \leq 1 \quad \forall i \in \mathcal{N}$.

The total bandwidth for transmission is divided into F frequency slots and the total time duration into T timeslots. A time-frequency slot is also called a resource block (RB) [25, section 6.2.3]. We assume that a VUE can transmit its packet using a single RB. Each VUE wants to broadcast a safety message to the VUEs in the corresponding set $\mathcal{R}$ within T timeslots. Hence, the latency constraint and time-slot duration determines T. Given a reliability constraint and the statistics of the small-scale fading, we can compute a SINR threshold γ^{T} such that packets are guaranteed to be received with the required error probability if the average received SINR is equal or greater than γ^{T} [2, Lemma 1].

We assume that a centralized controller schedules and power control all VUEs. A base station (BS) or a VUE can act as the centralized controller. We also assume that the average channel power gain (i.e., pathloss and large-scale fading) between the VUEs are known to the centralized controller. The small-scale fading can vary on a very short time scale, on the order of milliseconds, while changes in pathloss and large-scale fading are typically small for 100 ms, even at highway speeds. It is therefore more reasonable to assume knowledge of average channel power gains (slow CSI) than instantaneous channel gains (fast CSI). The pathloss and large-scale fading is measured by the individual VUEs and reported to the centralized controller.

B. ACI MODEL

The ACI caused by a transmitter depends mainly upon the power amplifier, the coding and modulation scheme, and clipping threshold [26]. In [27], the authors propose a two-stage low pass FIR filter method to reduce ACI in V2V communication. However, in order to find out a standard ACI model for single carrier frequency division multiple access (SCFDMA) signal, we did extensive simulations and the result for 1% clipping threshold is shown as blue colored curve in Fig. 3. The red-colored step curve in the same figure shows the SCFDMA ACI averaged over each frequency slot. The black step curve in Fig. 3 is the ACI mask specified for uplink by 3GPP [28], which is incidentally quite similar to the IEEE 802.11p mask [29].

A parameter named adjacent channel interference ratio (ACIR) is widely used to measure the ACI [30, section 17.9]. As illustrated in Fig. 2, ACIR is defined as the ratio between the average in-band received power from interferer k to the average received out of band power from interferer k's signal in the frequency band allocated for transmitter i. Let $\mathbf{A} \in \mathbb{R}^{F \times F}$ be the element-wise inverse ACIR matrix, i.e., $A_{f'f}$ is the ratio between the received power on the frequency slot f and the received power on the frequency slot f', when a transmitter sends a packet on frequency slot f'. Observe that $\mathbf{A}$ is a Toeplitz matrix. The mask specified by 3GPP [28] is as follows,

$$A_{f'f} = \begin{cases} 1, & f' = f \\ 10^{-3}, & 1 \leq |f' - f| \leq 4 \\ 10^{-4.5}, & \text{otherwise} \end{cases} \quad (1)$$

TABLE 1. Key mathematical symbols.

| Symbol	Definition
Parameters	
N	Number of VUEs
F	Number of frequency slots
T	Number of timeslots
$\mathcal{T}_j$	Set of intended transmitters for VUE j
$\mathcal{R}_i$	Set of intended receivers for VUE i
$A_{f',f}$	ACI from frequency slot f' to frequency slot f
$P^{\max}$	Maximum transmit power of a VUE
γ^{T}	SINR threshold to declare a link as successful
σ^2	Noise variance in an RB
Variables	
$P_{i,t}$	Transmit power of VUE i on an RB in timeslot t
$H_{i,j}$	Average channel power gain from VUE i to VUE j
$X_{i,f,t}$	Indicate if VUE i is scheduled to transmit in RB (f,t)
$Y_{j,f,t}$	Indicate if VUE j receives packet successfully in RB (f,t)
$\Upsilon_{i,j,t}$	SINR of the packet from VUE i to VUE j in timeslot t
$\Gamma_{j,f,t}$	SINR of the packet received by VUE j in RB (f,t)
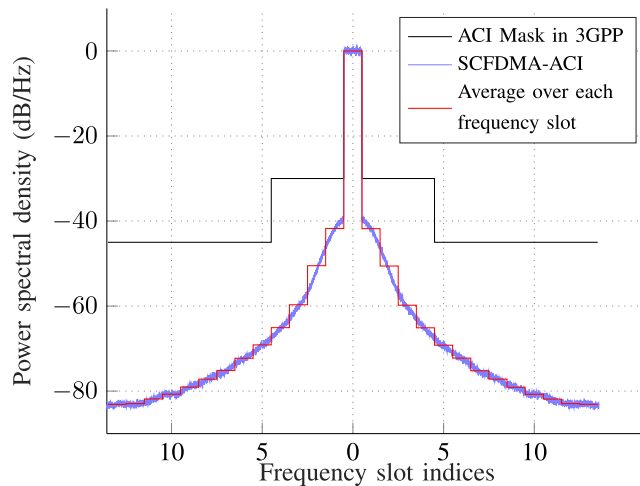
FIGURE 3. Inverse ACIR model.

The scenario $f' = f$ in the above equation implies that VUEs are allocated within the same RB, in which case the interference would be CCI instead of ACI.

III. JOINT SCHEDULING AND POWER CONTROL
A. CONSTRAINT FORMULATION
In this section we make the constraint on transmit power and scheduling mathematically precise. The objective is to maximize the number of successful links, which is done indirectly by introducing SINR constraints on as many possible desired links, i.e., the links $\{(i,j) : i \in \mathcal{N}, j \in \mathcal{R}_i\}$.

1) TRANSMIT POWER CONSTRAINT
We define the matrix $\mathbf{P} \in \mathbb{R}^{N \times T}$ where $P_{i,t}$ is the transmit power of VUE i, if scheduled in timeslot t. The value of $P_{i,t}$ is constrained by the maximum transmit power of a VUE $P^{\max}$ in an RB, i.e.,

$$0 \le P_{i,t} \le P^{\max} \quad \forall\, i,t \qquad (2)$$

2) SINR CONSTRAINT
Let us define $\Gamma \in \{0,1\}^{N \times F \times T}$ with $\Gamma_{j,f,t}$ as the received SINR of VUE j in RB (f,t), which can be computed as

$$\Gamma_{j,f,t} = \frac{S_{j,f,t}}{\sigma^2 + I_{j,f,t}}, \qquad (3)$$

where $S_{j,f,t}$ is the desired signal power, σ^2 is the noise variance, and $I_{j,f,t}$ is the interference power. We show how to compute the signal and interference powers in Section III-A.4 below. We note that focusing on the SINR of a certain receiving VUE j in an RB (f,t) allows us to state the joint scheduling and power control problem as an MIQCP problem, whereas a formulation using the SINR for specific transmitter-receiver pair would result in an harder problem as shown in Appendix A.

The SINR constraint for a successful link, i.e., $\Gamma_{j,f,t} \ge \gamma^{\mathrm{T}}$, can be rewritten as $S_{j,f,t} \ge \gamma^{\mathrm{T}}(\sigma^2 + I_{j,f,t})$, or equivalently

$$S_{j,f,t}(1 + \gamma^{\mathrm{T}}) \ge \gamma^{\mathrm{T}}(\sigma^2 + I_{j,f,t} + S_{j,f,t}) \qquad (4)$$

which in turn is equivalent to

$$S_{j,f,t} - \bar{\gamma}^{\mathrm{T}}(I_{j,f,t} + S_{j,f,t}) \ge \bar{\gamma}^{\mathrm{T}}\sigma^2, \qquad (5)$$

where $\bar{\gamma}^{\mathrm{T}} \triangleq \gamma^{\mathrm{T}}/(1 + \gamma^{\mathrm{T}})$. However, it might not be possible to fulfill this condition for all receivers j in all RBs (f,t). To select which combinations of j, f, and t to enforce this condition, we use the matrix $\mathbf{Y} \in \{0,1\}^{N \times F \times T}$, where

$$Y_{j,f,t} \triangleq \begin{cases} 1, & \text{(5) is enforced} \\ 0, & \text{otherwise} \end{cases} \qquad (6)$$

We can combine (5) and (6) into a single constraint as

$$S_{j,f,t} - \bar{\gamma}^{\mathrm{T}}(I_{j,f,t} + S_{j,f,t}) \ge \bar{\gamma}^{\mathrm{T}}\sigma^2 - \eta(1 - Y_{j,f,t}) \quad \forall j,f,t \quad (7)$$

where η is a sufficiently large number to make (7) hold whenever $Y_{j,f,t} = 0$, regardless of the schedule and power allocation. It is not hard to show that $\eta = \bar{\gamma}^{\mathrm{T}}(NP^{\max} + \sigma^2)$ is sufficient.

3) SCHEDULING CONSTRAINTS
Let $\mathbf{X} \in \{0,1\}^{N \times F \times T}$ be the scheduling matrix defined as

$$X_{i,f,t} \triangleq \begin{cases} 1, & \text{VUE } i \text{ is scheduled in RB } (f,t) \\ 0, & \text{otherwise} \end{cases} \qquad (8)$$

We limit a VUE scheduling to at most one RB in a timeslot, since scheduling in multiple RBs in a timeslot reduces available transmit power in an RB, and spreads interference across multiple RBs. Hence we add the following constraint,

$$\sum_{f=1}^{F} X_{i,f,t} \le 1 \quad \forall i,t. \qquad (9)$$

Recall that VUE j is interested in decoding packets from the VUEs in the set $\mathcal{T}_j$. If we set $Y_{j,f,t} = 1$, we want the SINR for receiver VUE j in RB (f,t) to be above γ^{T} for a transmitter VUE in $\mathcal{T}_j$. It then makes sense to not to allow more than one

VUE in $\mathcal{T}_j$ to transmit in RB (f, t), which is enforced by the following constraint,

$$\sum_{i \in \mathcal{T}_j} X_{i,f,t} \leq 1 + N(1 - Y_{j,f,t}) \quad \forall j, f, t. \tag{10}$$

Note that the above constraint is always satisfied when $Y_{j,f,t} = 0$, since $|\mathcal{T}_j| \leq N$. However, when $Y_{j,f,t} = 1$ then (10) implies that at most one VUE in $\mathcal{T}_j$ can transmit in RB (f, t) and CCI can therefore only be due to VUEs in the set $\mathcal{N} \setminus \mathcal{T}_j$, a fact that is used in (12) below.

4) COMPUTATION OF $S_{j,f,t}$ AND $I_{j,f,t}$

It follows from the scheduling constraints (9) and (10) that the desired signal power $S_{j,f,t}$ and interference power $I_{j,f,t}$ needed in the SINR constraint (7) can be computed as

$$S_{j,f,t} = \sum_{i \in \mathcal{T}_j} X_{i,f,t} P_{i,t} H_{i,j}, \tag{11}$$

$$I_{j,f,t} = \sum_{k \in \mathcal{N} \setminus \mathcal{T}_j} X_{k,f,t} P_{k,t} H_{k,j}$$
$$+ \sum_{\substack{f'=1 \\ f' \neq f}}^{F} \sum_{k \in \mathcal{N}} A_{f',f} X_{k,f',t} P_{k,t} H_{k,j}, \tag{12}$$

Note that the first term in (12) is CCI from VUEs not in $\mathcal{T}_j$ and that the second term is ACI from all transmitting VUEs.

B. PROBLEM FORMULATION

A link is defined as a transmitter-receiver pair (i, j), and we say that the link (i, j) is successful if at least one transmission from VUE i to VUE j is successful during the scheduling interval, i.e., that the SINR condition (5) is satisfied for at least one RB (f, t) where $f \in \{1, 2, \ldots, F\}$ and $t \in \{1, 2, \ldots, T\}$. We introduce the matrix $\mathbf{Z} \in \{0, 1\}^{N \times N}$, where, for all i, j,

$$Z_{i,j} \triangleq \min\{1, \sum_{t=1}^{T} \sum_{f=1}^{F} X_{i,f,t} Y_{j,f,t}\} \tag{13}$$

$$= \begin{cases} 1, & \text{link } (i, j) \text{ is successful} \\ 0, & \text{otherwise} \end{cases} \tag{14}$$

where the minimum in (13) is required to not to count successful links between VUE i and VUE j more than once.

The overall goal is to maximize the number of connected VUE pairs, i.e., to maximize the objective function

$$J(\mathbf{X}, \mathbf{Y}, \mathbf{P}) \triangleq \sum_{i=1}^{N} \sum_{\substack{j=1 \\ j \neq i}}^{N} Z_{i,j} \tag{15}$$

subject to the constraints (10), (9), (2), (7), and (13). However, since J is nonlinear with respect to the binary matrices $\mathbf{X}$ and $\mathbf{Y}$, direct optimization of J is cumbersome. We therefore formulate an equivalent optimization problem which is simpler to solve. To this end, let us define two auxiliary matrices

$\mathbf{V} \in \mathbb{R}^{N \times N \times F \times T}$ and $\mathbf{W} \in \mathbb{R}^{N \times N}$, where, for all i, j,

$$V_{i,j,f,t} \in \{v \in \mathbb{R} : v \leq X_{i,f,t}, v \leq Y_{j,f,t}\}, \tag{16}$$

$$W_{i,j} \in \{w \in \mathbb{R} : w \leq 1, w \leq \sum_{t=1}^{T} \sum_{f=1}^{F} V_{i,j,f,t}\}. \tag{17}$$

Now, for any fixed $\mathbf{X}, \mathbf{Y}$, it follows from (16) that

$$V_{i,j,f,t}^{\star} = \max V_{i,j,f,t} = \min\{X_{i,f,t}, Y_{j,f,t}\} = X_{i,f,t} Y_{j,f,t}. \tag{18}$$

The last equality in the above equation follows from the fact that both $X_{i,f,t}$ and $Y_{j,f,t}$ are Boolean. Moreover, it follows from (17) and (13) that if $V_{i,j,f,t} = V_{i,j,f,t}^{\star}$, then

$$\max W_{i,j} = \min\{1, \sum_{t=1}^{T} \sum_{f=1}^{F} V_{i,j,f,t}^{\star}\} = Z_{i,j}. \tag{19}$$

Hence, for any fixed $\mathbf{X}, \mathbf{Y}, \mathbf{P}$ we can compute $J(\mathbf{X}, \mathbf{Y}, \mathbf{P})$ as the optimal value of objective of

$$J(\mathbf{X}, \mathbf{Y}, \mathbf{P}) = \max_{\mathbf{V}, \mathbf{W}} \sum_{i=1}^{N} \sum_{\substack{j=1 \\ j \neq i}}^{N} W_{i,j}$$
$$\text{s.t } (16), (17) \tag{20a}$$

Putting everything together, we arrive at the optimization problem

$$\max_{\mathbf{P}, \mathbf{X}, \mathbf{Y}, \mathbf{V}, \mathbf{W}} \sum_{i=1}^{N} \sum_{j \in \mathcal{R}_i} W_{i,j} \tag{21a}$$

s.t.

$$\sum_{i \in \mathcal{T}_j} X_{i,f,t} P_{i,t} H_{i,j} - \bar{\gamma}^{\mathrm{T}} \sum_{f'=1}^{F} \sum_{k=1}^{N} A_{f',f} X_{k,f',t} P_{k,t} H_{k,j} \geq \bar{\gamma}^{\mathrm{T}} \sigma^2$$
$$- \bar{\gamma}^{\mathrm{T}} (N P^{\max} + \sigma^2)(1 - Y_{j,f,t}) \quad \forall j, f, t \tag{21b}$$

$$W_{i,j} \leq \sum_{t=1}^{T} \sum_{f=1}^{F} V_{i,j,f,t} \quad \forall i, j \tag{21c}$$

$$W_{i,j} \leq 1 \quad \forall i, j \tag{21d}$$

$$V_{i,j,f,t} \leq X_{i,f,t} \quad \forall i, j, f, t \tag{21e}$$

$$V_{i,j,f,t} \leq Y_{j,f,t} \quad \forall i, j, f, t \tag{21f}$$

$$\sum_{i \in \mathcal{T}_j} X_{i,f,t} \leq 1 + N(1 - Y_{j,f,t}) \quad \forall j, f, t \tag{21g}$$

$$\sum_{f=1}^{F} X_{i,f,t} \leq 1 \quad \forall i, t \tag{21h}$$

$$0 \leq P_{i,t} \leq P^{\max} \quad \forall i, t \tag{21i}$$

$$\mathbf{X}, \mathbf{Y} \in \{0, 1\}^{N \times F \times T} \tag{21j}$$

$$\mathbf{P} \in \mathbb{R}^{N \times T} \tag{21k}$$

$$\mathbf{V} \in \mathbb{R}^{N \times N \times F \times T} \tag{21l}$$

$$\mathbf{W} \in \mathbb{R}^{N \times N} \tag{21m}$$

Here are some of the key observations regarding the above problem formulation:

(i) We see that the problem (21) has linear objective and linear constraints except the constraint (21b), which is quadratic. We call such a problem an MIQCP problem. Moreover, the problem (21) is noncovex even after relaxing the Boolean constrains for $\mathbf{X}$ and $\mathbf{Y}$ as proved in Appendix B. Since there are $2NFT$ Boolean variables and $(NT + N^2FT + N^2)$ continuous variables in our power control problem formulation, we see that the worst-case computational complexity is $\mathcal{O}(\frac{(NT+N^2FT+N^2)^3 2^{2NFT}}{\log(NT+N^2FT+N^2)})$. The complexity 2^{2NFT} is due to fixing $2NFT$ Boolean variables, and the complexity $\frac{(NT+N^2FT+N^2)^3}{\log(NT+N^2FT+N^2)}$ is for solving each of the resulting linear programming (LP) problem using an interior point method [31].

(ii) The problem formulation (21) can be translated into a scheduling alone problem by fixing all power values $P_{i,t}$. The resulting problem is a BLP problem, with worst case computational complexity $\mathcal{O}(\frac{(N^2FT+N^2)^3 2^{2NFT}}{\log(N^2FT+N^2)})$.

(iii) The problem formulation (21) can be translated into a power control alone problem for an arbitrary scheduling matrix $\mathbf{X}$. That is, we fix the scheduling matrix $\mathbf{X}$ and optimize over $\mathbf{P}$ with the following modified objective function,

$$\max_{\mathbf{P},\mathbf{Y},\mathbf{V},\mathbf{W}} \sum_{i=1}^{N}\sum_{j\in\mathcal{R}_i} W_{i,j} - \beta \sum_{t=1}^{T}\sum_{i=1}^{N} P_{i,t}, \quad (22)$$

where β is the weight of the total power consumption in the objective, in order to achieve our secondary goal of minimizing the total power consumption. We note that if $\beta \leq 1/(NTP^{\max})$, then the sum power minimization does not affect our primary objective of maximizing the total number of successful links. Furthermore, we can change constraint (21c) to $W_{i,j} \leq \sum_{(f,t):X_{i,f,t}=1} Y_{j,f,t}$, thereby avoiding the need for variable $\mathbf{V}$.

Observe that the problem of finding the optimal power values is NP-hard as proved in [11, Lemma 1], and the worst-case computational complexity is $\mathcal{O}(\frac{(N^2+NT)^3 2^{NFT}}{\log(N^2+NT)})$.

(iv) The problem formulation (21) allows for full-duplex communication, i.e., a VUE can simultaneously transmit and receive. However, half-duplex communication can be enforced by adding the following constraint,[1]

$$Y_{i,j,f,t} \leq (1 - X_{j,f',t}) \quad \forall i, j, f, f', t \quad (23)$$

(v) The optimization problem in (21) can be reformulated to maximize the minimum number of successful links
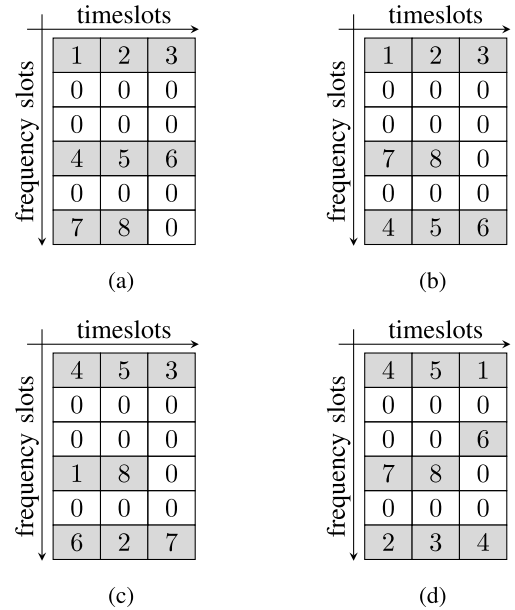
FIGURE 4. Example of scheduling 8 VUEs in 6 × 3 RBs. VUEs are placed on a convoy with inter vehicular distance 48.6 m. (a) BIS ($w = 1$). (b) BIS ($w = 2$). (c) Heuristic scheduling. (d) Optimal scheduling.

for a VUE, instead of the total number of successful links. By doing this, at least L^* links are guaranteed to be successful for any VUE. This is done by changing the objective function in (21a) to

$$L^* = \max_{\mathbf{P},\mathbf{X},\mathbf{Y},\mathbf{V},\mathbf{W},L} L \quad (24)$$

and adding an extra constraint,

$$\sum_{\substack{j=1\\j\neq i}}^{N} Z_{i,j} \geq L \quad \forall i \quad (25)$$

(vi) Furthermore, we note that the problem formulation in (21) can also be used for unicast communication by setting $\mathcal{R}_i$ to a singleton set containing the intended receiver of VUE i, for all $i \in \mathcal{N}$. This way, we are reducing the number of constraints in the problem and, therefore, also the computational complexity.

IV. SCHEDULING ALGORITHMS
For the scheduling problem, without considering any power control, we set the transmit power of all VUEs to $\bar{P}$, where, $0 \leq \bar{P} \leq P^{\max}$. For the sake of scheduling all available RBs, we define VUE 0 as a dummy VUE with zero transmit power. Hence, scheduling VUE 0 to an RB indicate that no VUE is scheduled in that RB.

Let us define the matrix $\mathbf{U} \in \{0, 1, \ldots, N\}^{F \times T}$ to represent scheduled VUEs in an $F \times T$ RBs matrix. That is, $U_{f,t}$ is the VUE index scheduled in RB (f, t). Fundamentally, scheduling is the process of allocating VUEs in available RBs, which is equivalent to populating the $\mathbf{U}$ matrix with appropriate VUE indices, as illustrated in Fig. 4. Once we

Algorithm 1 Block Interleaver Scheduler (BIS)
Input: $\{N, F, T, w\}$
Output: X
1: $\tilde{N} = \min\{\lfloor NT/2 \rfloor, N, FT\}$
2: $\tilde{F} = \lceil \tilde{N}/T \rceil$
3: Compute **f** and **n** from (27) and (29)
4: $\mathbf{f}' = \Pi(\mathbf{f}, w)$
5: $\mathbf{U} = \mathbf{0}^{F \times T}$
6: $k = 1$
7: **for** $l = 1 : |\mathbf{f}'|$ **do**
8:     $f' = f'_l$
9:     **for** $t = 1 : T$ **do**
10:         **if** $k \leq |\mathbf{n}|$ **then**
11:             $U_{f',t} = n_k$
12:             $k = k + 1$
13:         **end if**
14:     **end for**
15: **end for**
16: Compute **X** from **U** using (26)

have computed **U**, the matrix **X** can be computed as follows,

$$X_{i,f,t} = \begin{cases} 1, & U_{f,t} = i \\ 0, & \text{otherwise} \end{cases}. \quad (26)$$

A. BLOCK INTERLEAVER SCHEDULER (BIS)
The algorithm is summarized in Algorithm 1. The approach here is to insert each VUE index exactly once in **U**. Clearly, this is impossible if $N > FT$, i.e., when there are more VUEs than available RBs. For the time being, we assume that $N \leq FT$ and treat the $N > FT$ case later in this Section. Moreover, we assume that $N > T$, since the scheduling problem is trivial otherwise; we can simply schedule the VUEs in separate timeslots, which removes all ACI and CCI interferences.

If $N > T$, then we need to multiplex VUEs in frequency, which results in ACI. To reduce the ACI problem, we strive to use as few frequency slots as possible and to space the frequency slots as far apart as possible. Since T VUEs can be scheduled per frequency slot, the smallest required number of frequency slots is $\tilde{F} = \lceil N/T \rceil$. Clearly, $\tilde{F} \leq F$, since we assume that $N \leq FT$. The selected frequency slots are put in the vector $\mathbf{f} \in \{1, 2, \ldots, F\}^{\tilde{F}}$. For BIS, we use the frequency slots

$$f_k = 1 + \left\lceil (k-1)\frac{F-1}{\tilde{F}-1} \right\rceil, \quad k = 1, 2, \ldots, \tilde{F}. \quad (27)$$

We note that $f_1 = 1 < f_2 < \cdots < f_{\tilde{F}} = F$, and it can be shown that (27) maximizes the minimum distance between any two consecutive frequency slots, i.e., maximizes

$$\min_{l \in \{1,2,\ldots,\tilde{F}-1\}} |f_{l+1} - f_l|. \quad (28)$$

We initialize $\mathbf{U} = \mathbf{0}^{F \times T}$. Then, given **f**, BIS starts by filling the rows of **U** in the natural way, i.e., row f_1 with VUE indices $1, 2, \ldots, T$, row f_2 with indices $T+1, T+2, \ldots, 2T$, and

so on. To (possibly) improve the scheduler, the nonzero rows of **U** are then permuted with a block interleaver Π; which is equivalent to permuting **f** with the block interleaver Π before filling in the rows of **U**.

Now we explain the block interleaver Π used to permute **f**. Our block interleaver is same as the one specified in 3GPP [25, section 5.1.4.2.1]. We define $\mathbf{f}' = \Pi(\mathbf{f}, w)$ as the output $\mathbf{f}'$ of a block interleaver with width $w \in \mathbb{N}$ and input vector **f**. The block interleaver writes **f** row-wise in a matrix with width w, padding with zeros if necessary, then reads $\mathbf{f}'$ from the matrix column-wise ignoring zeros. Observe that if $w = 1$, then the block interleaver output is same as the input, i.e., $\mathbf{f}' = \mathbf{f}$. The width of the block interleaver w is an input to this algorithm.

As an example, when $N = 8, F = 6, T = 3, w = 1$, we compute $\mathbf{f}' = \mathbf{f} = [1, 4, 6]$, and schedule VUEs accordingly as shown in Fig. 4 (a). Similarly, Fig. 4 (b) shows the result when $w = 2$ and the computed $\mathbf{f}' = [1, 6, 4]$. We present the results for various values of w in Section VII-B.

Now let us treat the case when $N > FT$. One way to handle this case is to schedule only $\tilde{N} \leq FT$ of the N VUEs. For BIS, we put the selected VUEs in the vector $\mathbf{n} \in \{1, 2, \ldots, N\}^{\tilde{N}}$, where

$$n_k = 1 + \left\lceil (k-1)\frac{N-1}{\tilde{N}-1} \right\rceil, \quad k = 1, 2, \ldots, \tilde{N}. \quad (29)$$

We note that if $\tilde{N} = N$, then $\mathbf{n} = [1, 2, \ldots, N]$. Hence, the two cases $N \leq FT$ and $N > FT$ can be unified by letting $\tilde{N} = \min\{N, FT\}$ and $\tilde{F} = \lceil \tilde{N}/T \rceil$.

However, if $T = 1$, then it is never advantageous to schedule more than $\lfloor N/2 \rfloor$ VUEs in the half-duplex case. To understand why, we note that since we have $\tilde{N}$ transmitters and $N - \tilde{N}$ receivers, the maximum number of successful links we can ever hope for is $\tilde{N}(N - \tilde{N}) = (N/2)^2 - (\tilde{N} - N/2)^2$, which is maximized when $\tilde{N} = \min\{\lfloor N/2 \rfloor, F\}$. Scheduling more than $\lfloor N/2 \rfloor$ VUEs does not increase the number of possible links (due to half-duplex criteria), but increase ACI. The final, unifying, calculation of $\tilde{N}$ in Algorithm 1 is therefore $\tilde{N} = \min\{\lfloor TN/2 \rfloor, N, FT\}$ and $\tilde{F} = \lceil \tilde{N}/T \rceil$, which covers all cases of N, F, and T.

B. HEURISTIC SCHEDULING ALGORITHM
The approach taken here is to loop through all RBs and schedule either a real or dummy VUE to each RB. The scheduling decision is taken in a greedy fashion. That is, we strive to schedule the best possible VUE to the RB under the assumption that the schedule for all previous RBs is fixed. The resulting schedule can schedule a VUE, zero, one, or multiple times, as opposed to BIS, which schedules all real VUEs exactly once (if there are enough RBs, $FT \geq N$ and $T > 1$).

The heuristic algorithm is executed in two steps: 1) Determine the RB scheduling order, 2) Use this order to sequentially visit the RBs and schedule VUEs.

Algorithm 2.1 Computation of Scheduling Order **f**

Input: $\{F, \mathbf{A}\}$

Output: f

1: $f_1 = 1$
2: $\mathcal{F} = \{2, 3, \ldots, F\}$
3: **for** $l = 2 : F$ **do**
4: $\quad \mathcal{G} = \arg\min_{f \in \mathcal{F}} \sum_{l'=1}^{l-1} A_{f_{l'}, f}$
5: $\quad f_l = \max\left\{\arg\max_{f \in \mathcal{G}} \sum_{l'=1}^{l-1} |f - f_{l'}|\right\}$
6: $\quad \mathcal{F} = \mathcal{F} \setminus f_l$
7: **end for**

Algorithm 2.2 Heuristic Scheduling Algorithm

Input: $\{N, F, T, \mathbf{H}, \mathbf{A}, \mathbf{P}, \gamma^{\mathrm{T}}, \sigma^2\}$

Output: X

1: $\mathbf{X} = \mathbf{0}^{N \times F \times T}, \quad \mathbf{U} = \mathbf{0}^{F \times T}$
2: Compute **f** using Algorithm 2.1
3: // Schedule RBs in the order specified by **f**
4: **for** $l = 1 : F$ **do**
5: $\quad f = f_l$
6: $\quad$ **for** $t = 1 : T$ **do**
7: $\quad\quad$ // Schedule VUE in RB (f, t)
8: $\quad\quad$ **for** $i = 0 : N$ **do**
9: $\quad\quad\quad U_{f,t} = i$
10: $\quad\quad\quad$ Compute **X** from **U** using (26)
11: $\quad\quad\quad$ Compute **Z** for **X** using (13)
12: $\quad\quad\quad s_i = \sum_{m=1}^{N} \sum_{j \in \mathcal{R}_m} Z_{m,j}$
13: $\quad\quad$ **end for**
14: $\quad\quad U_{f,t} = \arg\max_i \{s_i\}$
15: $\quad$ **end for**
16: **end for**
17: Compute **X** from **U** using (26)

Now we explain the first step, i.e., the procedure to compute the scheduling order **f** for frequency slots. We note that **f** is a permutation of $\{1, 2, \ldots, F\}$, which can be chosen in $F!$ possible ways. We compute **f** using a greedy algorithm as shown in Algorithm 2.1. That is, while constructing **f**, our priority is to spread out the consecutive scheduling frequency slots in order to minimize the received ACI. Therefore, in each iteration, we are scheduling a frequency slot with minimum received ACI from all the scheduled frequency slots. Therefore, we always start scheduling from the first frequency slot, i.e., $f_1 = 1$, then we find out the next frequency slot f_2 as the unscheduled frequency slot with minimum received ACI from f_1. We repeat this process until all frequency slots are chosen. Finding the frequency slot with minimum received ACI from all the scheduled frequency slots is actually impossible, since we do not know yet which VUE is going to be scheduled in the RBs and its transmit power. Therefore, we compute the ACI in an unscheduled frequency slot by assuming unit transmit power and unit channel gain from all interferers. If there are multiple unscheduled frequency slots with the same minimum affected ACI, then the frequency slot having maximum average distance from all the scheduled frequency slots is chosen. If there is still a tie, then the max value is chosen as shown in Algorithm 2.1, line 5. This way, $f_2 = F$ is ensured for a typical ACIR model.

Next we explain the second step, i.e., finding out the VUE to schedule in an RB. The algorithm is shown in Algorithm 2.2. Given an RB to schedule, first we compute the total number of successful links upon scheduling each VUE in the chosen RB, we then pick the VUE which would maximize this quantity. Observe that VUE 0 (the dummy VUE) can be scheduled to an RB, which, of course, means that no real VUE is scheduled. Counting the number of *for* loops and the operations on lines 11 and 12 in Algorithm 2.2, we see that the heuristic scheduling is a polynomial time algorithm with the worst case computational complexity $\mathcal{O}(NFT(FT + N^2))$.

The result of the scheduling when $N = 8, F = 6$, and $T = 3$, is shown in Fig. 4 (c), when VUEs are placed on a one lane road, with equal distances d_{avg} (refer

to Table 2) to the neighboring VUEs, and by assuming zero shadow loss. Note that in this example VUE 4 is scheduled twice.

V. HEURISTIC POWER CONTROL

Since the exponentially increasing worst-case complexity of optimal power control is problematic in practice for large networks, we propose a heuristic power control algorithm which has polynomial time computational complexity. The proposed heuristic power control algorithm is an extension of our previous work on power control [11] and the work of Wang et al. [32]. All those previous works assumes $T = 1$, whereas our proposed algorithm finds a power control solution for any value of T. The algorithm is described in Algorithm 3.

The SINR $\Upsilon_{i,j,t}$ of a link (i, j) during the timeslot t is computed as follows,

$$\Upsilon_{i,j,t} = \frac{\sum_{f=1}^{F} X_{i,f,t} P_{i,t} H_{i,j}}{\sigma^2 + \sum_{f=1}^{F} \sum_{f'=1}^{F} \sum_{\substack{k=1 \\ k \neq i}}^{N} X_{i,f,t} A_{f',f} X_{k,f',t} P_{k,t} H_{k,j}}. \quad (30)$$

The derivation of the above equation is explained in Appendix A. A link (i, j) is successful if and only if its SINR is greater than or equals to γ^{T} on any timeslot, i.e., $\Upsilon_{i,j,t} \geq \gamma^{\mathrm{T}}$ for any $t \in \{1, 2, \ldots, T\}$. Our goal is to find the optimal transmit power value for each VUE in each timeslot in order to maximize the total number of successful links. The algorithm is an iterative algorithm involving two steps in each iteration. Since it may not be possible to ensure success for all links, our first step is to find the set of candidate links

$\mathcal{L}$. The second step is to compute the power values $P_{i,t}$ for all VUEs in all timeslots in order to maximize the number of successful links in $\mathcal{L}$. Therefore, we update both $\mathcal{L}$ and $P_{i,t}$ $\forall i, t$ in each iteration. We terminate the algorithm, when we observe that all the links in $\mathcal{L}$ are achieving the SINR target γ^{T}.

Now we explain the first step, i.e., the computation of $\mathcal{L}$ on each iteration. In the first iteration, we initialize $\mathcal{L}$ to the set of all links, and in the subsequent iterations we remove some of the links from $\mathcal{L}$, thereby making $\mathcal{L}$ a nonincreasing set over iterations. We initialize all VUEs transmit power to P^{init}, i.e., $P_{i,t} = P^{\mathrm{init}} \forall i, t$. We then define the variable $\tilde{P}_{i,j,t}$ as the required transmit power of VUE i during the timeslot t in an iteration, so that the link (i, j) would be successful in the next iteration, under the assumption that the interference remains constant. The value of $\tilde{P}_{i,j,t}$ is computed in each iteration as shown in Algorithm 3, line 8. If the required power for a link (i, j) is more than P^{max}, i.e., $\tilde{P}_{i,j,t} > P^{\mathrm{max}} \forall t$, then the link (i, j) is declared as a broken link. The set of broken links $\mathcal{B}$ in an iteration is computed in Algorithm 3, line 9. We find out repeatedly broken links over many iterations and remove them from the set $\mathcal{L}$ (line 16).

In order to find the repeatedly broken links, a counter $C_{i,j}$ is set to count the number of iterations at which the link (i, j) gets broken. We remove the link (i, j) from $\mathcal{L}$ once $C_{i,j}$ reaches above a threshold C^{max}, i.e, $C_{i,j} > C^{\mathrm{max}}$. We observe that, the algorithm shows improved performance as we increase C^{max}. However, higher values of C^{max} increases computational complexity due to more number of iterations. Moreover, the initial transmit power P^{init} plays a crucial role in this algorithm. A higher value of P^{init} leads to more number of broken links in the first iteration itself, meanwhile lower values lead to a slow convergence of the algorithm. By simulations, we observe that $P^{\mathrm{init}} = P^{\mathrm{max}}/10$ is a reasonable value for P^{init}.

Next we explain the second step, i.e., the computation of power values $P_{i,t}$ $\forall t$, in each iteration. We compute the power values of each VUE independently. In the following, we therefore explain the power value computation of an arbitrary VUE i for all timeslots $t \in \{1, 2, \ldots, T\}$. Let us define the set $\bar{\mathcal{R}}_i$ as the set of intended receivers in $\mathcal{L} \setminus \mathcal{B}$ for the transmitting VUE i, as computed in Algorithm 3, line 13. Our goal is to make the received SINR of all the links from VUE i to VUEs in $\bar{\mathcal{R}}_i$ equal to or greater than γ^{T} in the next iteration, i.e., $\Upsilon_{i,j,t} \geq \gamma^{\mathrm{T}} \forall j \in \bar{\mathcal{R}}_i$. Therefore, we compute $P_{i,t}$ $\forall t$, such that the SINR values of all the links in $\mathcal{L} \setminus \mathcal{B}$ are greater or equal to γ^{T} on at least one of the timeslots in the next iteration, under the assumption that the interference remains constant.

Furthermore, in order to minimize the interference to other links, we would consider allocating power to a VUE in as few number of timeslots as possible. Therefore, the power allocation to VUE i involves two steps. The first step is to decide the optimal timeslot $t^\star$ to allocate power, and the second step is to compute the power value for the chosen timeslot $t^\star$. We compute $t^\star$ as the timeslot at which VUE i can serve

---

Algorithm 3 Heuristic Power Control

Input: $\{N, F, T, P^{\mathrm{init}}, P^{\mathrm{max}}, \mathbf{X}, \mathbf{H}, \mathbf{A}, \gamma^{\mathrm{T}}, \sigma^2\}$
Output: P

1: $P_{i,t} = P^{\mathrm{init}}$ $\forall i, t$
2: $\mathbf{C} = \mathbf{0}^{N \times N}$

　// set of candidate links
3: $\mathcal{L} = \{(i, j) : \sum_{t=1}^{T} \sum_{f=1}^{F} X_{i,f,t} > 0, j \in \mathcal{R}_i\}$

　// scheduled time-slots for VUE i
4: $\bar{\mathcal{T}}_i = \{t : \sum_{f=1}^{F} X_{i,f,t} > 0\}$ $\forall i$

5: Compute SINR $\Upsilon_{i,j,t}$ $\forall i, j, t$ using (30)
6: **while** $\exists (i, j) \in \mathcal{L}$ s.t. $\Upsilon_{i,j,t} < \gamma^{\mathrm{T}}$ $\forall t$ **do**
7: 　// Compute the required power and broken links $\mathcal{B}$
8: 　$\tilde{P}_{i,j,t} = \frac{\gamma^{\mathrm{T}}}{\Upsilon_{i,j,t}} P_{i,t}$ $\forall (i, j) \in \mathcal{L}, t \in \bar{\mathcal{T}}_i$
9: 　$\mathcal{B} = \{(i, j) : \tilde{P}_{i,j,t} > P^{\mathrm{max}}$ $\forall t \in \bar{\mathcal{T}}_i\}$
10: 　// Increment $C_{i,j}$ and update $\mathcal{L}$
11: 　$C_{i,j} = C_{i,j} + 1$ $\forall (i, j) \in \mathcal{B}$
12: 　$\mathcal{L} = \mathcal{L} \setminus \{(i, j) : C_{i,j} > C^{\mathrm{max}}\}$
13: 　$\bar{\mathcal{R}}_i = \{j : (i, j) \in \mathcal{L} \setminus \mathcal{B}\}$ $\forall i$
14: 　// Compute power values
15: 　$P_{i,t} = 0$ $\forall i, t$
16: 　**for** $i = 1 : N$ **do**
17: 　　**while** $\bar{\mathcal{R}}_i \neq \emptyset$ **do**
18: 　　　$\mathcal{K}_t = \{\tilde{P}_{i,j,t} : \tilde{P}_{i,j,t} \leq P^{\mathrm{max}}, j \in \bar{\mathcal{R}}_i\} \forall t \in \bar{\mathcal{T}}_i$
19: 　　　$t^\star = \arg\max_{t \in \bar{\mathcal{T}}_i} |\mathcal{K}_t|$
20: 　　　$P_{i,t^\star} = \max \mathcal{K}_{t^\star}$
21: 　　　$\bar{\mathcal{R}}_i^\star = \{j : P_{i,t^\star} \geq \tilde{P}_{i,j,t^\star}\}$
22: 　　　$\bar{\mathcal{R}}_i = \bar{\mathcal{R}}_i \setminus \bar{\mathcal{R}}_i^\star$
23: 　　**end while**
24: 　**end for**
25: 　Compute SINR $\Upsilon_{i,j,t}$ $\forall i, j, t$ using (30) with updated power values
26: **end while**

---

the maximum number of intended receivers in $\bar{\mathcal{R}}_i$. For this purpose, we first compute $\mathcal{K}_t$ as the set of transmit powers for VUE i that are required to serve the receivers in $\bar{\mathcal{R}}_i$ and do not exceed P^{max}, as shown in Algorithm 3, line 18. Clearly, the cardinality of this set, i.e., $|\mathcal{K}_t|$, is the number of receivers that can be served during timeslot t in the next iteration. Therefore, $t^\star$ is computed as the timeslot t that maximizes $|\mathcal{K}_t|$ (i.e., $t^\star = \arg\max_t |\mathcal{K}_t|$), and ties are broken arbitrarily. We compute the power value $P_{i,t^\star}$ as the maximum value in $\mathcal{K}_{t^\star}$ (which is less than P^{max}), as shown in Algorithm 3, line 20. Then we compute the set of receivers $\bar{\mathcal{R}}_i^\star$ which are served by the allocated power $P_{i,t^\star}$, and remove those from $\bar{\mathcal{R}}_i$, thereby making the set $\bar{\mathcal{R}}_i$ as the set of VUEs not yet served. We repeat these two steps until the allocated transmit power $P_{i,t}$ is greater or equal to the required transmit power $\tilde{P}_{i,j,t}$ on at least one of the timeslot t, for all receivers in $\bar{\mathcal{R}}_i$.

The algorithm is convergent since maximum number of iterations possible in line 6 is $C^{\max} |\mathcal{L}|$ as proved in Lemma 1 in Appendix C. Counting the number of iterations in lines 6, 16, 17 and computation of $\Upsilon_{i,j,t}$ in algorithm 7, we see that the heuristic power control is a polynomial time algorithm with worst case computational complexity $\mathcal{O}(C^{\max} N^6 T)$.

VI. COMPUTATIONAL COMPLEXITY AND OVERHEAD OF THE ALGORITHMS

A. COMPUTATIONAL COMPLEXITY

The computational complexity of various algorithms are compared in Table 3. Obviously, the maximum network size that can be handled depends on the computational resources of the centralized controller, and a VUE or a BS can act as a centralized controller. It is worth mentioning that typical self-driving algorithms require high computational capability and large storage [33], and future vehicles will be equipped with powerful processing units and memory [34], therefore, it might not be such a big difference in computational resources between BS and vehicles. However, the exponential computational complexity of finding an optimal solution will be prohibtive for sufficiently large networks. For such large networks, we suggest either to use the proposed heuristic algorithms or to segment the network into smaller networks as discussed in Section IX.

B. NUMERICAL ISSUES IN THE SOLVER

As a practical note, we observe that ACI-aware scheduling and power control problem might be numerically sensitive due to the presence of both large and small coefficients in the constraints. This numerical sensitivity is due to the high dynamic range of ACIR values and V2V channel values, which result in an even higher dynamic range for the ACI values (i.e., the dynamic range of $A_{f',f} H_{i,j}$). This could result in numerical problems, since 1) the solver tolerate slight infeasibility,[2] 2) finite-precision arithmetic results in round-off errors.[3] Furthermore, the round-off errors make basic mathematical operations (like addition, multiplication) to lose their associative property. These are some fundamental problems for any optimization solver, and techniques to overcome these are hard and out of scope of this paper. Therefore, quantifying the optimality gap due to numerical sensitivity is not treated in this paper. However, a brute-force search for optimal scheduling for smaller networks show zero optimality gap, which gives us hope (but no proof) that the optimality gap is small for larger networks as well.

---

[2]For illustration, consider the following BLP problem: max $x_1 + x_2$ such that $a_1 x_1 + a_2 x_2 \leq a_1$ and $x_1, x_2 \in \{0, 1\}$. Assuming $a_1, a_2 > 0$, a truly optimal solution is $(x_1, x_2) = (1, 0)$. However, if $a_1/a_2 \geq 10^{12}$, then a typical optimization solver returns an infeasible solution $(x_1, x_2) = (1, 1)$ due to the solvers tolerance for infeasibility.

[3]For instance, assuming floating-point arithmetic, suppose we add a small number α to a large number β, then subtract the large number β from the summation (i.e., $(\alpha + \beta) - \beta$). The result could be zero due round-off errors in the floating point representation. [35]

C. OVERHEAD OF THE ALGORITHMS

There are mainly three overheads for the algorithms as follows,

1) Measuring CSI: Each VUE has to periodically broadcast a pilot signal to allow the other VUEs to measure the channel gains.

2) Gathering CSI: The centralized controller need to know the CSI (slowly varying channel gain) between any pair of VUEs (i.e., $N(N-1)$ channel gains). Therefore, each VUE needs to periodically report (to the centralized controller) the measured channel values to the other VUEs. If the channel between any pair of VUEs is reciprocal, then the centralized controller requires $N(N-1)/2$ CSI values. Typically large-scale fading varies over distances on the order of 40λ, where λ is the wavelength, while small-scale fading varies over the distances on the order of $\lambda/2$ [36]. Therefore, for VUEs travelling at highway speed and communicating in the 6 GHz band, CSI reporting every 10–100 ms should be sufficient.

3) Disseminating schedule and power allocation: The centralized controller has to communicate the schedule and power value to all VUEs before every new scheduling interval.

All the above three types of overhead are applicable for all algorithms considered in this paper, except BIS which does not require CSI.

VII. PERFORMANCE EVALUATION

A. SCENARIO AND PARAMETERS

For the simulation purpose, we consider a platooning scenario, where N VUEs are distributed on a convoy, as used in the realtime vehicular channel measurements done in [37]. The distance between any two adjacent VUEs, d, follows a shifted exponential distribution, with the minimum distance $d_{\min}$ and the average distance d_{avg} [38]–[41]. That is, the probability density function of d is given as,

$$f(d) = \begin{cases} \dfrac{1}{d_{\text{avg}} - d_{\min}} \exp(-\dfrac{d - d_{\min}}{d_{\text{avg}} - d_{\min}}), & d \geq d_{\min} \\ 0, & \text{otherwise} \end{cases} \quad (31)$$

Following the recommendation by 3GPP [42, section A.1.2] for freeway scenario, d_{avg} is set to 48.6 m, which corresponds to 2.5 seconds for a vehicular speed of 70 km/h. We note that the mobility is less of a concern for the time scale of the problem under study. Typically, the latency requirement is less than 100 ms, over which time the slow CSI (i.e., pathloss and shadowing) typically does not vary significantly, even in a highway speed. Fast channel variations (i.e., small-scale fading) is accounted for in the calculation of γ^{T}. That is, γ^{T} is computed from the small-scale fading statistics (not its realizations) and the reliability constraint, see [2, Lemma 1] for details. In other words, there is no need for an explicit mobility model to assess performance of the scheduling and power control algorithms in this paper.

We adopt the channel model from [37], which is a model based on the real-time measurements of V2V links at carrier

Parameter	Value
ACIR model	3GPP mask
γ^{T}	5 dB
$P^{\max}$	24 dBm
P^{init}	$P^{\max}/10$
PL_0	63.3 dB
n	1.77
d_0	10 m
σ_1	3.1 dB
Penetration Loss	10 dB per obstructing VUE
σ^2	-95.2 dBm
d_{avg}	48.6 m
$d_{\min}$	10 m
β	$1/(NP^{\max})$
η	$\gamma^{\mathrm{T}}(NP^{\max} + \sigma^2)$
$C^{\max}$	100

frequency 5.2 GHz in a highway scenario. We note that the measurements in [37] are consistent with the measurements done in [43]–[45]. The pathloss in dB for a distance d is computed as,

$$\mathrm{PL}(d) = \mathrm{PL}_0 + 10n \log_{10}(d/d_0) + X_{\sigma_1} \quad (32)$$

where n is the pathloss exponent, PL_0 is the pathloss at a reference distance d_0, and X_{σ_1} represents the shadowing effect modeled as a zero-mean Gaussian random variable with standard deviation σ_1. The values of the channel parameters are taken from [37] (shown in Table 2), which is based upon real-time measurements in a highway scenario. The penetration loss caused by multiple obstructing vehicles has not been fully understood by research community yet. However, the penetration loss caused by a single vehicle has been widely studied. Measurements show that an obstructing truck causes 12–13 dB [4], a bus 15–20 dB [6], a van 20 dB [5], and a car 10 dB [3] penetration loss.

To summarize, there is no widely accepted, measurement-based model for the penetration loss of multiple vehicles available in the literature. For simulations purpose, we therefore simply assume that each blocking vehicle introduce an additional attenuation of 10 dB. The noise variance is -95.2 dBm and $P^{\max}$ is 24 dBm as per 3GPP recommendations [28]. We assume that $d_{\min} = 10$ m and that $\gamma^{\mathrm{T}} = 5$ dB is sufficient for a transmission to be declared as successful (i.e., that the error probability averaged over the small-scale fading is sufficiently small). Additionally, we fix $C^{\max} = 100$, which is found to be a reasonable value for the heuristic power control algorithm. For the simulation purpose, the set $\mathcal{T}_j$ is chosen as the closest $\min(N-1, FT-1)$ VUEs to VUE j based on the distance between the VUEs.

We present results for half-duplex communication in this paper. Moreover, for simulation purposes, we use the ACI mask specified for uplink by 3GPP [28], since LTE uplink physical layer is a possible candidate for vehicular communication [1] upon introduction of Cellular-V2X in release 14 of the LTE standard [46]. Simulation results for full-duplex and the SCFDMA ACI model is available in the report [47], but is not presented here due to space constraints.

B. SIMULATION RESULTS
To measure performance, we use the following metrics

$$Z_i = \sum_{j \in \mathcal{R}_i} Z_{i,j}, \quad (33)$$

$$\bar{Z}_i = \mathrm{E}[Z_i], \quad (34)$$

$$\bar{Z} = \frac{1}{N} \sum_{i=1}^{N} \bar{Z}_i, \quad (35)$$

where Z_i is the number of successful links from VUE i, when VUE i is transmitting a packet to all VUEs in set $\mathcal{R}_i$. The quantity $\bar{Z}_i$ is the expected value of Z_i, where the expectation is taken over the random quantities in the experiment, i.e., the inter-VUE distances and shadow fading. Finally, $\bar{Z}$ is the number of successful links for a VUE, averaged across all VUEs. In other words, the metric $\bar{Z}$ can be interpreted as the average number of receiving VUEs that can decode a packet from a certain VUE. Clearly, we would like to ensure that $\bar{Z}$ is sufficiently large to support the application in mind. However, to specify this minimum acceptable value of $\bar{Z}$ is out of scope of this paper.

We use Gurobi solver [48] for finding optimal scheduling and optimal power values, as described in ii and iii in Section III-B respectively. However, an optimization toolbox might not return optimal solution due to the fundamental numerical issues as discussed in Section VI-B. Therefore, we refer the solutions provided by the solver as "Optimal scheduling (numerical)" and "Optimal power (numerical)," in Figs. 5–7.

Since the block interleaver width w is an input parameter to BIS, we considered a class of BIS with all possible $w \in \{1, 2, \ldots, \tilde{F} - 1\}$. We present here the results for the optimal w which maximizes $\bar{Z}$ under the assumption of equal transmit powers, shown as the blue curves marked with triangles in Fig. 5. The corresponding w for BIS is shown as an extra x label on top of Figs. 5(a)–(c), and we do not vary w with respect to the power control algorithms.

To the best of our knowledge, there is no multicast scheduling algorithm with the objective of maximizing the connectivity in the current literature, even though the routing algorithms in V2V have been widely studies [33], [49]. In [50], authors propose a multicast scheduling algorithm to improve Quality of Services (QoS). As a benchmark, we simulate the proposed algorithm in [50] after modifying the objective function to maximize the connectivity (instead of improving QoS), and plotted as violet curve marked with plus in Figs. 5-6. The proposed scheduling algorithm in [50] is an ACI-unaware algorithm, and performance seems to be comparable with BIS (optimized w). However, [50] assumes channel knowledge, whereas BIS does not require any channel information.

In Fig. 5, we present the result for various values of F, T, N, and various scheduling and power control algorithms. In Figs. 5(a)–(c), we present the results for equal power, i.e., when all VUEs transmit with the same power $\bar{P}$. We know that the performance improves as $\bar{P}$ increases, since
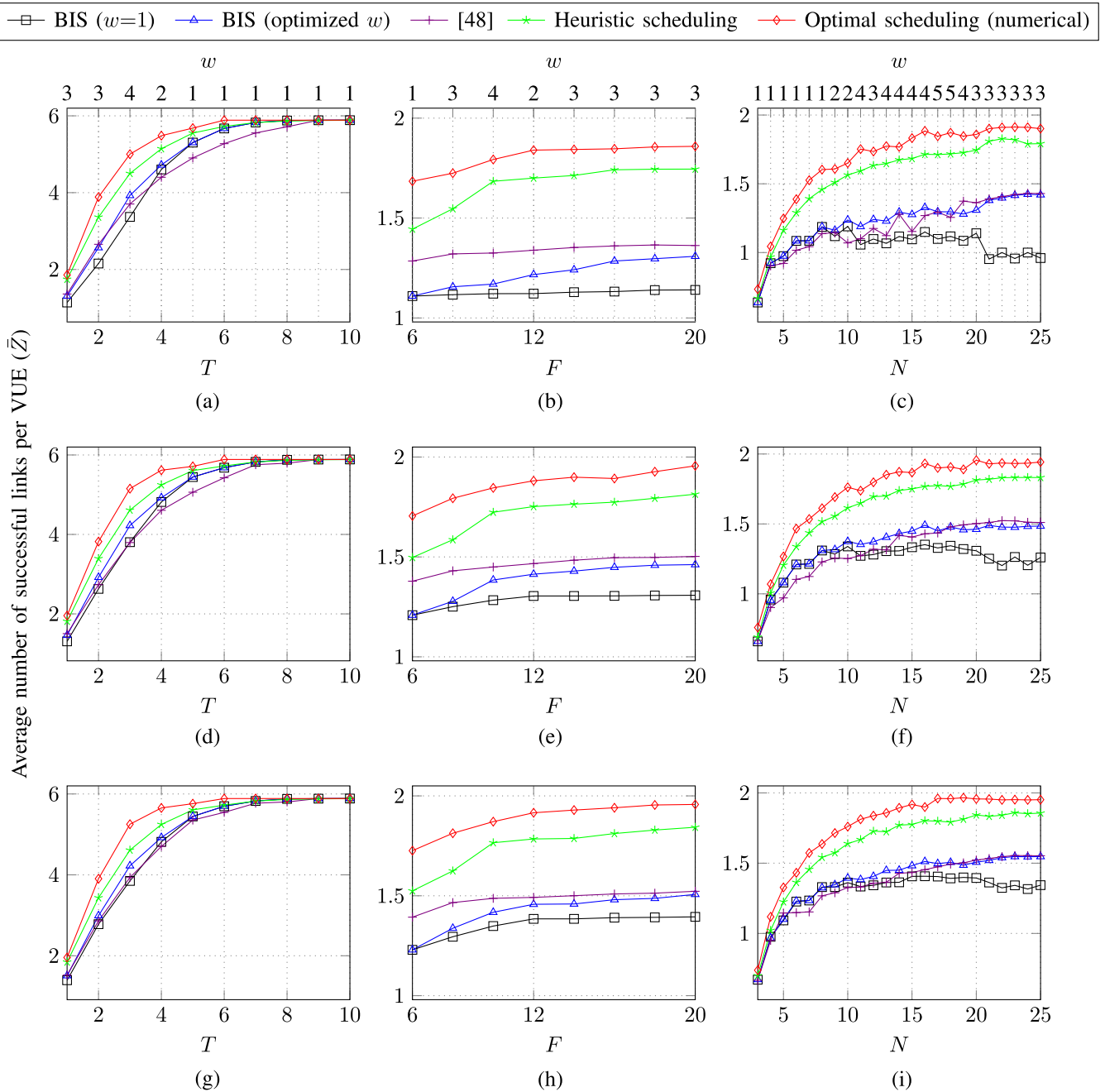
FIGURE 5. Average number of successful links for a VUE ($\bar{Z}$) for various scheduling algorithms. (a) Equal Power ($F = 20$; $N = 20$). (b) Equal Power ($T = 1$; $N = 20$). (c) Equal Power ($F = 20$; $T = 1$). (d) Heuristic Power ($F = 20$; $N = 20$). (e) Heuristic Power ($T = 1$; $N = 20$). (f) Heuristic Power ($F = 20$; $T = 1$). (g) Optimal power (numerical) ($F = 20$; $N = 20$). (h) Optimal power (numerical) ($T = 1$; $N = 20$). (i) Optimal power (numerical) ($F = 20$; $T = 1$).

both the signal power and the interference power are linear functions of $\bar{P}$, thereby making the SINR an increasing function of $\bar{P}$. Therefore, we set $\bar{P} = P^{\max}$. In Fig. 5(a), we plot $\bar{Z}$ by varying T for a fixed F and N. The results in Fig. 5(a) clearly show that $\bar{Z}$ is severely limited by ACI when many VUEs must be multiplexed in frequency, i.e., when T is small compared to N. This motivates the search for scheduling and power control methods to mitigate the ACI problem in this

situation. We also observe that $\bar{Z}$ remains essentially constant for $T \geq 10$ due to limitations by noise power.

One way to limit the effect of ACI would be to increase F (for a fixed N and T) to allow for larger spacing of VUEs in frequency. However, the results in Fig. 5(b) show that $\bar{Z}$ is only slowly increasing with F. On the other hand, Fig. 5(b) shows that significant gains can be achieved by more advanced scheduling than using a BIS.
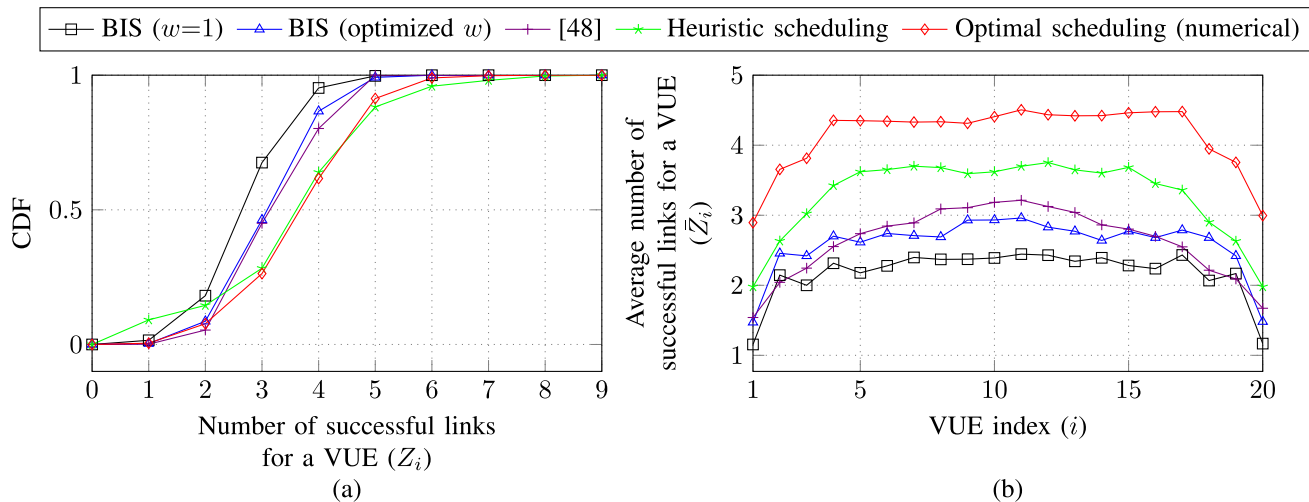
FIGURE 6. Fairness comparison of number of successful links for equal power ($F = 20$; $T = 2$; $N = 20$). (a) Number of successful links for a VUE (Z_i). (b) VUE index (i).

TABLE 3. Summary of compared algorithms (Performance compared when $N = 20$, $F = 20$, and $T = 2$).

| Line Style	Scheduling	Power control	Worst-Case Complexity	Performance ($\bar{Z}$)	Performance ($\bar{Z}$) (no ACI case)	Execution time (seconds)
—□—	BIS ($w = 1$)	Equal power	$\mathcal{O}(FT + F)$	2.16	3.50	0.11
—△—	BIS (optimized w)	Equal power	$\mathcal{O}(F(FT + F))$	2.57	3.50	0.14
—+—	[48]	Equal power	$\mathcal{O}(N^2 FT)$	2.66	4.29	5.21
—✳—	Heuristic scheduling	Equal power	$\mathcal{O}(NFT(FT + N^2))$	3.36	3.82	7.44
—◇—	Optimal scheduling (numerical)	Equal power	$\mathcal{O}\left(\frac{(N^2 FT + N^2)^3 2^{2NFT}}{\log(N^2 FT + N^2)}\right)$	3.89	4.79	1.36×10^4
—□—	BIS ($w = 1$)	Heuristic power control	$\mathcal{O}((FT + F)C^{\max} N^6 T)$	2.63	3.50	11.46
—□—	BIS ($w = 1$)	Optimal power (numerical)	$\mathcal{O}\left((FT + F)\frac{(N^2 + NT)^3 2^{NFT}}{\log(N^2 + NT)}\right)$	2.78	3.50	1.52×10^4
	Optimal joint scheduling and power control (numerical)		$\mathcal{O}\left(\frac{(NT + N^2 FT + N^2)^3 2^{2NFT}}{\log(NT + N^2 FT + N^2)}\right)$	4.58	4.79	3.11×10^4

Moreover, for a fixed T and F, we see in Fig. 5(c) that $\bar{Z}$ is increasing with N, at least for the more advanced schedulers. This might be surprising at first sight; however, this effect is not unreasonable, since more receivers become available for each transmission when N increases. In other words, the number of terms in the double sum in (35) increases, which tends to increase $\bar{Z}$. However, the performance flattens out for higher values of N (i.e., $N \geq 20$). This is because as the network size grows, the links between VUEs that are blocked by several other VUEs become noise limited due to the penetration loss of the blocking VUEs. In this case scheduling and power control cannot improve the performance anymore.

As seen in Figs. 5(d)–(i), power control improves performance, but, in general, the gains are marginal for advanced schedulers. The performance gain is more significant for the BIS scheduler compared to the more advanced schedulers. This can be explained by the fact that a suboptimal schedule can be corrected to some degree by power control. Indeed, assigning zero or a very low power to a VUE effectively changes the schedule for that VUE. For instance, that the

performance for BIS with $w = 1$ for large N is significantly improved with power control, as seen in Fig. 5(f) and Fig. 5(i).

It is, of course, possible to iterate between scheduling and power control. However, we have observed that this gives only marginal improvement at the price of significantly increased computational complexity. Due to space constraints, detailed results are not presented here.

In Fig. 6(a), we plot CDF of the number of successful links for a VUE, Z_i defined in (33), for fairness comparison between various scheduling algorithms. We observe that, BIS and [50] perform better in terms of fairness than the heuristic scheduling algorithm, in the sense that its corresponding CDF is more steep in Fig. 6(a). In Fig. 6(b), we plot the average number of successful links for each VUE, $\bar{Z}_i$ defined in (34), in a convoy of 20 VUEs. We note that VUEs in the middle of the convoy are able to successfully broadcast their packets to more number of VUEs than the VUEs on the edge of the convoy, which is logical since the VUEs in the middle have more number of close-by neighbors. Moreover, even if BIS ($w = 1$) is more fair, the per-VUE performance is uniformly worse compared to the other algorithms.
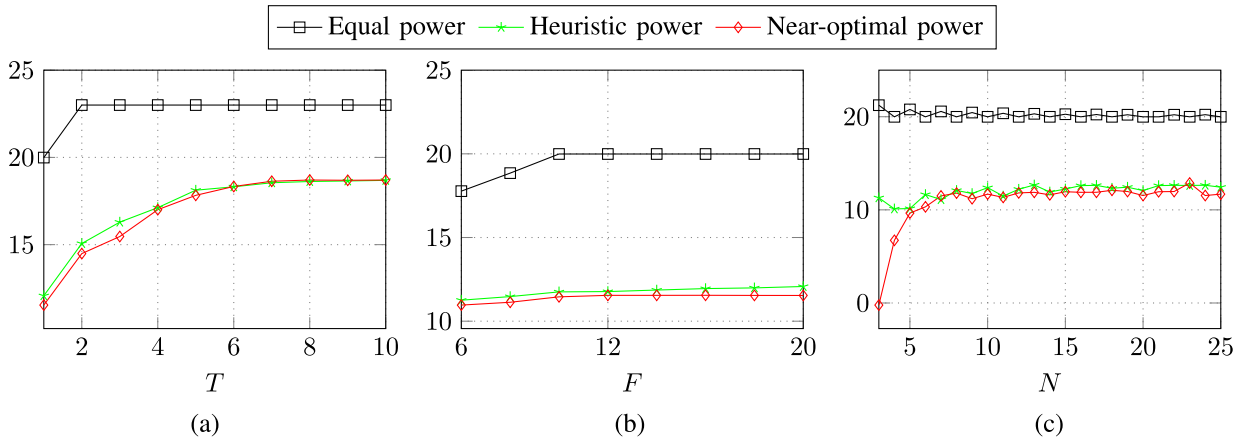
FIGURE 7. Average transmit power per VUE (dBm) for various power control algorithms for BIS ($w = 1$). (a) ($F = 20$; $N = 20$). (b) ($T = 1$; $N = 20$). (c) ($F = 20$; $T = 1$).

Except for the naturally lower $\bar{Z}_i$ for the edge VUEs, all algorithms are seen to be approximately fair.

In Table 3, we summarize the computational complexity of the studied algorithms and the performance for a benchmark case when $N = 20$, $F = 20$, and $T = 2$. We also show the result for optimal scheduling and power control (numerical) upon solving MIQCP problem (21). The result for scheduling algorithms (i.e., first 5 rows in Table 3 are given for the equal power control, and results for the power control algorithms (i.e., 6th and 7th rows) are given for the scheduling algorithm BIS ($w = 1$). The last column in the table is the performance for no ACI case, i.e., $\mathcal{A}_{f',f} = 0$, $\forall f \neq f'$. For no ACI case, a non-overlapping scheduling with maximum transmit power for each VUE would yield the best performance. However, due to the half-duplex assumption, careful splitting the VUEs into transmitter and receiver roles in each timeslot yields improved performance. Therefore, the improvement seen by more advanced schedulers in the last column in the table is due to this effect. Also, we note that the optimal joint scheduling and power control can more or less nullify the negative impact of ACI since its performance with and without ACI are comparable. The last column in Table 3 shows the execution time in core-seconds for each algorithm for our implementation in a 16 core machine with Intel 2650v3 processor and 64 GB RAM. However, it should be noted that the execution time is heavily dependent on the computational hardware and software optimization. Hence, the execution time values in Table 3 are only indicative.

It should be stressed that a scheduling and power control method that is only concerned with CCI and ignores ACI would be trivial in the case when full-duplex communication is possible and when $N \leq FT$: scheduling all VUEs in non-overlapping RBs and allocate maximum transmit power P^{max} to all VUEs would be thought to be optimum since no CCI would occur. For half-duplex, the case is a bit more complicated. If VUE i is scheduled in timeslot t, then we should avoid scheduling any other VUEs in $\mathcal{R}_i$ in the same timeslot. If this is possible, the schedule is optimal

(if ACI can be ignored). Indeed, all schedules in Fig. 4 (a) are optimum (if ACI can be ignored) when all VUEs want to communicate with their two closest neighbors on each side. However, we note that ignoring ACI can lead to considerable performance loss, as the case is for the BIS ($w = 1$) scheduler in Fig. 5.

In Fig. 7, we plot the average transmitter power values for various power control algorithms, upon fixing the scheduling algorithm as BIS with $w = 1$. We observe that our proposed heuristic power control algorithm uses less transmit power compared to equal power, and close to the transmit power used by optimal power control.

For detailed results on full-duplex and SCFDMA ACI, interested readers are directed to our report in the archive [47]. We observe that the optimal scheduling algorithm show significant performance improvement for full-duplex communication scenarios when ACIR equals to 3GPP mask. Moreover, the simulation results in the report [47] show that the order of performance for the algorithms is the same as the one presented here, regardless of the ACI model. We also plot the average transmit power values for various scheduling algorithms in [47], and observe the similar trends. Additionally, the MATLAB code used for the simulation is shared on github [51].

VIII. CONCLUSIONS

This paper studies performance of V2V broadcast communication by focusing more upon the scenario where CCI is limited due to the non-overlapping scheduling of VUEs. From the results presented in this paper, which are for half-duplex communication, we can draw the following conclusions.

1) Performance is mainly limited by ACI due to near-far situation in V2V networks when VUEs are multiplexed in frequency.
2) Performance is heavily dependent on scheduling and power allocation.

3) In general, scheduling with fixed and equal transmit powers is more effective in improving performance than subsequent power control.

4) To find a schedule and power allocation to maximize performance can be stated as the nonconvex mixed integer quadratic constrained programming (MIQCP) problem in (21).

5) To find a schedule to maximize performance for a fixed power allocation can be stated as a Boolean linear programming (BLP) problem found by fixing **P** to a constant matrix in (21).

6) The heuristic scheduling algorithm for a fixed power allocation defined in Algorithm 2.2 has significantly lower complexity than the BLP program and performs significantly better than the baseline block-interleaver scheduler defined in Algorithm 1.

7) To find a power allocation to maximize performance for a fixed schedule can be stated as an MILP problem found by replacing the objective in (21) with (22) and fixing **X**.

8) The heuristic power allocation algorithm for a fixed schedule defined in Algorithm 3 achieve similar performance as the solution to the MILP problem, but at a significantly lower computational complexity.

IX. FUTURE WORKS

We note that the scalability is an issue for all the algorithms presented in this paper, since a centralized controller may not exist for a larger network and computing optimal solution becomes hard. One possible approach to reduce the computational complexity is to split the network into smaller networks and do the scheduling and power control for each smaller network independently. The splitting should be done in a ''soft'' manner to avoid the edge effects. For example, suppose N VUEs are divided into M groups and that each group has a centralized controller. We assume that the grouping is done such that VUEs in group m want to communicate with VUEs found in groups $m - 1$, m and $m + 1$ and that transmissions from group m cause relatively less interference to VUEs in groups $m \pm 2, m \pm 3, \ldots$, etc. We partition the groups into 3 partitions, i.e., the groups $\{1, 4, 7, \ldots\}$ is called partition 1, groups $\{2, 5, 8, \ldots\}$ as partition 2, and groups $\{3, 6, 9, \ldots\}$ as partition 3. Since interference is limited between the groups within a partition, groups in each partition can reuse resources, e.g., groups $\{1, 4, 7, \ldots\}$ can reuse the same timeslot. However, since there can be interference between partitions, we use time-division multiplexing to separate partitions, e.g., the VUEs in partition 1 are scheduled in timeslots $\{1, 3, 5, \ldots\}$, partition 2 VUEs in timeslots $\{2, 4, 6, \ldots\}$, etc. In this way, inter-partition interference (CCI and ACI) is avoided. The analysis of this scheme is not done yet, but will be presented in a future publication.

Additional future works would involve devising scheduling and power control algorithms for V2V communication networks in a decentralized manner (i.e., without a centralized controller), and to address the numerical sensitivity

issues. A study upon the sensitivity of the parameters and the possibilities for multihop communication are also topics for future works.

APPENDIX A
JOINT SCHEDULING AND POWER CONTROL PROBLEM FORMULATION BY FOCUSING ON TRANSMITTER-RECEIVER LINKS

Let us define $\Upsilon \in \mathbb{R}^{N \times N \times T}$ with $\Upsilon_{i,j,t}$ being the SINR during timeslot t for the link from VUE i to VUE j, i.e., transmitter-receiver link (i, j). The value of $\Upsilon_{i,j,t}$ can be computed as follows,

$$\Upsilon_{i,j,t} = \frac{\sum_{f=1}^{F} X_{i,f,t} P_{i,t} H_{i,j}}{\sigma^2 + \sum_{f=1}^{F} \sum_{f'=1}^{F} \sum_{\substack{k=1 \\ k \neq i}}^{N} X_{i,f,t} A_{f',f} X_{k,f',t} P_{k,t} H_{k,j}} \quad (36)$$

where σ^2 is the noise variance and $P_{i,t}$ is the transmit power of VUE i during timeslot t.

Now we explain each component of (36). Observe that $X_{i,f,t} P_{i,t} H_{i,j}$ in the numerator is the received signal power for the link (i, j) on RB (f, t), therefore, $\sum_{f} X_{i,f,t} P_{i,t} H_{i,j}$ is the total received signal power in timeslot t. Similarly $A_{f',f} X_{k,f',t} P_{k,t} H_{k,j}$ is the interference power received by VUE j on RB (f, t) from VUE k when VUE k is scheduled to transmit on RB (f', t). Similarly, $X_{i,f,t} A_{f',f} X_{k,f',t} P_{k,t} H_{k,j}$ is the same received interference power if VUE i is scheduled to transmit in RB (f, t). Therefore, $\sum_{f} \sum_{f'} \sum_{k \neq i} X_{i,f,t} A_{f',f} X_{k,f',t} P_{k,t} H_{k,j}$ is the total interference power received to the link (i, j) if VUE i is scheduled to transmit in any of the RBs in timeslot t.

However, translating the constraint for achieving SINR target, i.e., $\Upsilon_{i,j,t} \geq \gamma^{\mathrm{T}}$, we get the following constraint,

$$\sum_{f=1}^{F} X_{i,f,t} P_{i,t} H_{i,j}$$

$$- \gamma^{\mathrm{T}} \sum_{f=1}^{F} \sum_{f'=1}^{F} \sum_{\substack{k=1 \\ k \neq i}}^{N} X_{i,f,t} A_{f',f} X_{k,f',t} P_{k,t} H_{k,j} \geq \gamma^{\mathrm{T}} \sigma^2 \quad (37)$$

Observe that the above constraint is more complicated than a quadratic constraint. Moreover, we can simplify the above constraint only upto a Boolean quadratic constraint for a scheduling problem, upon fixing the power values $P_{i,t} \forall i, t$.

APPENDIX B
PROVING THE NONCONVEXITY OF (21b)

Let us represent (21b) as follows,

$$G(\mathbf{P}, \mathbf{X}, \mathbf{Y}) \leq 0 \quad (38)$$

where $G(\mathbf{P}, \mathbf{X}, \mathbf{Y})$ is defined as follows,

$$G(\mathbf{P}, \mathbf{X}, \mathbf{Y}) = -\sum_{i=1}^{N} X_{i,f,t} P_{i,t} H_{i,j}$$

$$+ \gamma^{\mathrm{T}} \sum_{\substack{f'=1 \\ f' \neq f}}^{F} \sum_{k=1}^{N} A_{f',f} X_{k,f',t} P_{k,t} H_{k,j}$$
$$+ \gamma^{\mathrm{T}} \sigma^2 - \gamma^{\mathrm{T}} (NP^{\max} + \sigma^2)(1 - Y_{j,f,t}) \quad (39)$$

We prove the nonconvexity of (21b) by proving that $G(\mathbf{P}, \mathbf{X}, \mathbf{Y})$ is nonconvex. We prove this by proving that the Hessian matrix of $G(\mathbf{P}, \mathbf{X}, \mathbf{Y})$ is not positive semidefinite, with respect to the two variables $x = X_{1,f,t}$ and $y = P_{1,t}$. The Hessian matrix of $G(\mathbf{P}, \mathbf{X}, \mathbf{Y})$ with respect to x and y is as follows,

$$\nabla^2 G = \begin{bmatrix} \dfrac{\partial^2 G}{\partial^2 x} & \dfrac{\partial^2 G}{\partial y \partial x} \\ \dfrac{\partial^2 G}{\partial x \partial y} & \dfrac{\partial^2 G}{\partial^2 y} \end{bmatrix} \quad (40)$$

However, observe that $\frac{\partial^2 G}{\partial^2 x} = \frac{\partial^2 G}{\partial^2 y} = 0$, and $\frac{\partial^2 G}{\partial x \partial y} = \frac{\partial^2 G}{\partial y \partial x}$ from (39). Therefore, the determinant of the above Hessian matrix is $\left| \nabla^2 G \right| = -(\frac{\partial^2 G}{\partial x \partial y})^2 \leq 0$. Since $\frac{\partial^2 G}{\partial x \partial y} \neq 0$ for some j, f, t, the corresponding determinant of the Hessian matrix is negative. Hence the function $G(\mathbf{P}, \mathbf{X}, \mathbf{Y})$ is nonconvex. This concludes the proof.

APPENDIX C
PROVING THE CONVERGENCE OF ALGORITHM 3

Lemma 1: The Algorithm 3 is convergent.

Proof: Observe that the set $\mathcal{L}$ is nonincreasing on each iteration. When the termination condition (Algorithm 3, line 6) is not satisfied, the set of broken links $\mathcal{B}$ is nonempty. This implies that, the counter $C_{i,j}$ is incremented for some $(i, j) \in \mathcal{L}$ in each iteration. Therefore, the maximum number of iterations possible before the set $\mathcal{L}$ becomes empty is $C^{\max} |\mathcal{L}|$. This concludes the proof. ∎

ACKNOWLEDGMENT

REFERENCES

[1] G. Araniti, C. Campolo, M. Condoluci, A. Iera, and A. Molinaro, "LTE for vehicular networking: A survey," *IEEE Commun. Mag.*, vol. 51, no. 5, pp. 148–157, May 2013.

[2] W. Sun, E. G. Ström, F. Brännström, K. C. Sou, and Y. Sui, "Radio resource management for D2D-based V2V communication," *IEEE Trans. Veh. Technol.*, vol. 65, no. 8, pp. 6636–6650, Aug. 2016.

[3] T. Abbas, K. Sjöberg, J. Karedal, and F. Tufvesson, "A measurement based shadow fading model for vehicle-to-vehicle network simulations," *Int. J. Antennas Propag.*, vol. 2015, Feb. 2015, Art. no. 190607.

[4] D. Vlastaras, T. Abbas, M. Nilsson, R. Whiton, M. Olbäck, and F. Tufvesson, "Impact of a truck as an obstacle on vehicle-to-vehicle communications in rural and highway scenarios," in *Proc. 6th Int. Symp. Wireless Veh. Commun. (WiVeC)*, Sep. 2014, pp. 1–6.

[5] R. Meireles, M. Boban, P. Steenkiste, O. Tonguz, and J. Barros, "Experimental study on the impact of vehicular obstructions in VANETs," in *Proc. IEEE Veh. Netw. Conf.*, Jersey City, NJ, USA, Dec. 2010, pp. 338–345.

[6] R. He, A. F. Molisch, F. Tufvesson, Z. Zhong, B. Ai, and T. Zhang, "Vehicle-to-vehicle propagation models with large vehicle obstructions," *IEEE Trans. Intell. Transp. Syst.*, vol. 15, no. 5, pp. 2237–2248, Oct. 2014.

[7] X. Hong, Z. Chen, C.-X. Wang, S. A. Vorobyov, and J. S. Thompson, "Cognitive radio networks: Interference cancellation and management techniques," *IEEE Trans. Veh. Technol.*, vol. 4, no. 4, pp. 76–84, Dec. 2009.

[8] W. Li, X. Ma, J. Wu, K. S. Trivedi, X.-L. Huang, and Q. Liu, "Analytical model and performance evaluation of long-term evolution for vehicle safety services," *IEEE Trans. Veh. Technol.*, vol. 66, no. 3, pp. 1926–1939, Mar. 2017.

[9] J. Zhou, R. Q. Hu, and Y. Qian, "Message scheduling and delivery with vehicular communication network infrastructure," in *Proc. IEEE Global Commun. Conf. (GLOBECOM)*, Atlanta, GA, USA, Dec. 2013, pp. 575–580.

[10] F. Zeng, R. Zhang, X. Cheng, and L. Yang, "Channel prediction based scheduling for data dissemination in VANETs," *IEEE Commun. Lett.*, vol. 21, no. 6, pp. 1409–1412, Jun. 2017.

[11] A. Hisham, W. Sun, E. G. Ström, and F. Brännström, "Power control for broadcast V2V communications with adjacent carrier interference effects," in *Proc. IEEE Int. Conf. Commun. (ICC)*, May 2016, pp. 1–6.

[12] H. Albasry, H. Zhu, and J. Wang, "The impact of in-band emission interference in D2D-enabled cellular networks," in *Proc. IEEE Global Commun. Conf.*, Dec. 2017, pp. 1–5.

[13] D. Li and Y. Liu, "In-band emission in LTE-A D2D: Impact and addressing schemes," in *Proc. IEEE 81st Veh. Technol. Conf.*, May 2015, pp. 1–5.

[14] V. Angelakis, S. Papadakis, V. A. Siris, and A. Traganitis, "Adjacent channel interference in 802.11a is harmful: Testbed validation of a simple quantification model," *IEEE Commun. Mag.*, vol. 49, no. 3, pp. 160–166, Mar. 2011.

[15] L. Wang, X. Qi, and K. Wu, "Embracing adjacent channel interference in next generation Wi-Fi networks," in *Proc. IEEE Int. Conf. Commun. (ICC)*, May 2016, pp. 1–6.

[16] A. Adya, P. Bahl, J. Padhye, A. Wolman, and L. Zhou, "A multi-radio unification protocol for IEEE 802.11 wireless networks," in *Proc. 1st Int. Conf. Broadband Netw.*, San Jose, CA, USA, Oct. 2004, pp. 344–354.

[17] J. Nachtigall, A. Zubow, and J. P. Redlich, "The impact of adjacent channel interference in multi-radio systems using IEEE 802.11," in *Proc. Int. Wireless Commun. Mobile Comput. Conf.*, Aug. 2008, pp. 874–881.

[18] W. Li, J. Chen, H. Long, and B. Wu, "Performance and analysis on LTE system under adjacent channel interference of broadcasting system," in *Proc. IEEE 12th Int. Conf. Comput. Inf. Technol.*, Oct. 2012, pp. 290–294.

[19] Q. Wang and X. Li, "Analysis of LTE FDD and TD-LTE combination network's interference," in *Proc. 2nd IEEE Int. Conf. Comput. Commun. (ICCC)*, Oct. 2016, pp. 2332–2336.

[20] J. Ribadeneira-Ramírez, G. Martínez, D. Gómez-Barquero, and N. Cardona, "Interference analysis between digital terrestrial television (DTT) and 4G LTE mobile networks in the digital dividend bands," *IEEE Trans. Broadcast.*, vol. 62, no. 1, pp. 24–34, Mar. 2016.

[21] "CEPT Report 40: Compatibility study for LTE and WiMAX operating within the bands 880-915 MHz/925-960 MHz and 1710-1785 MHz/1805-1880 MHz (900/1800 MHz bands)," CEPT Electron. Commun. Committee, Copenhagen, Denmark, Tech. Rep. CEPT 40, Nov. 2010. [Online]. Available: https://www.ecodocdb.dk/download/4ce187bc-3569/CEPTREP040.PDF

[22] K. Xia, Y. Wang, and D. Zhang, "Coexistence interference evaluation and analysis of LTE with 3D-MIMO system," in *Proc. IEEE 28th Annu. Int. Symp. Pers., Indoor, Mobile Radio Commun. (PIMRC)*, Oct. 2017, pp. 1–6.

[23] C. Campolo, A. Molinaro, and A. Vinel, "Understanding adjacent channel interference in multi-channel VANETs," in *Proc. IEEE Veh. Netw. Conf. (VNC)*, Dec. 2014, pp. 101–104.

[24] C. Campolo, C. Sommer, F. Dressler, and A. Molinaro, "On the impact of adjacent channel interference in multi-channel VANETs," in *Proc. IEEE Int. Conf. Commun. (ICC)*, May 2016, pp. 1–7

[25] *Evolved Universal Terrestrial Radio Access (E-UTRA); Physical Channels and Modulation*, document 36.211, 3rd Generation Partnership Project 3GPP, Mar. 2017. [Online]. Available: http://www.3gpp.org/ftp/Specs/archive/36_series/36.211

[26] T. Svensson and T. Eriksson, "On power amplifier efficiency with modulated signals," in *Proc. IEEE 71st Veh. Technol. Conf.*, May 2010, pp. 1–5.

[27] J. Almeida, M. Alam, J. Ferreira, and A. S. Oliveira, "Mitigating adjacent channel interference in vehicular communication systems," *Digit. Commun. Netw.*, vol. 2, no. 2, pp. 57–64, May 2016. [Online]. Available: http://www.sciencedirect.com/science/article/pii/S2352864816300104

[28] *Evolved Universal Terrestrial Radio Access (E-UTRA); Radio Frequency (RF) System Scenarios*, document TR 36.942, 3rd Generation Partnership Project (3GPP), Oct. 2014. [Online]. Available: http://www.3gpp.org/ftp/Specs/html-info/36942.htm

[29] *ISO/IEC/IEEE International Standard—Information Technology–Telecommunications and Information Exchange Between Systems Local and Metropolitan Area Networks–Specific Requirements Part 11: Wireless LAN Medium Access Control (MAC) and Physical Layer (PHY) Specifications*, Standard ISO/IEC/IEEE 8802-11:2018(E), Mar. 2018, pp. 1–6.

[30] E. Dahlman, S. Parkvall, and J. Skold, *4G: LTE/LTE-Advanced for Mobile Broadband*. New York, NY, USA: Oxford: Academic Press, 2011.

[31] F. A. Potra and S. J. Wright, "Interior-point methods," *J. Comput. Appl. Math.*, vol. 124, nos. 1–2, pp. 281–302, Jan. 2000.

[32] K. Wang, C. Chiasserini, J. Proakis, and R. Rao, "Joint scheduling and power control for multicasting in wireless ad hoc networks," in *Proc. IEEE 58th Veh. Technol. Conf.*, Orlando, FL, USA, Oct. 2003, pp. 2915–2920.

[33] W. Xu *et al.*, "Internet of vehicles in big data era," *IEEE/CAA J. Autom. Sinica*, vol. 5, no. 1, pp. 19–35, Jan. 2018.

[34] F. Yang, S. Wang, J. Li, Z. Liu, and Q. Sun, "An overview of Internet of vehicles," *China Commun.*, vol. 11, no. 10, pp. 1–15, Oct. 2014.

[35] W. Contributors. (2019). *IEEE 754-2008 Revision—Wikipedia, The Free Encyclopedia*. Accessed: Feb. 5, 2019. [Online]. Available: https://en.wikipedia.org/w/index.php?title=IEEE_754-2008_revision&ol% did=877917438

[36] A. F. Molisch, *Wireless Communication*, 2nd ed. Hoboken, NJ, USA: Wiley 2011.

[37] J. Karedal, N. Czink, A. Paier, F. Tufvesson, and A. F. Molisch, "Path loss modeling for vehicle-to-vehicle communications," *IEEE Trans. Veh. Technol.*, vol. 60, no. 1, pp. 323–328, Jan. 2011.

[38] K. Koufos and C. P. Dettmann, "Temporal correlation of interference in vehicular networks with shifted-exponential time Headways," *IEEE Wireless Commun. Lett.*, vol. 8, no. 1, pp. 189–192, Feb. 2019.

[39] D. Kong and X. Guo, "Analysis of vehicle headway distribution on multi-lane freeway considering car—Truck interaction," *Adv. Mech. Eng.*, vol. 8, no. 4, pp. 1–12, Apr. 2016. doi: 10.1177/1687814016646673.

[40] R. J. Cowan, "Useful headway models," *Transp. Res.*, vol. 9, no. 6, pp. 371–375, Dec. 1975. [Online]. Available: http://www.sciencedirect.com/science/article/pii/0041164775900088

[41] R. T. Luttinen, "Statistical analysis of vehicle time headways," Ph.D. dissertation, Dept. Built Environ., Aalto Univ., Helsinki, Finland, 1996. [Online]. Available: http://urn.fi/urn:nbn:fi:tkk-007970

[42] *Technical Specification Group Radio Access Network; Study on LTE-based V2X Services*, document 3rd Generation Partnership Project (3GPP), TR 36.885, Jun. 2016. [Online]. Available: http://www.3gpp.org/ftp/Specs/html-info/36885.htm

[43] T. Abbas, J. Nuckelt, T. Kürner, T. Zemen, C. F. Mecklenbräuker, and F. Tufvesson, "Simulation and measurement-based vehicle-to-vehicle channel characterization: Accuracy and constraint analysis," *IEEE Trans. Antennas Propag.*, vol. 63, no. 7, pp. 3208–3218, Jul. 2015.

[44] L. Cheng, B. E. Henty, F. Bai, and D. D. Stancil, "Highway and rural propagation channel modeling for vehicle-to-vehicle communications at 5.9 GHz," in *Proc. IEEE Antennas Propag. Soc. Int. Symp.*, Jul. 2008, pp. 1–4.

[45] J. Kunisch and J. Pamp, "Wideband car-to-car radio channel measurements and model at 5.9 GHz," in *Proc. IEEE 68th Veh. Technol. Conf.*, Sep. 2008, pp. 1–5.

[46] *Evolved Universal Terrestrial Radio Access (E-UTRA) and Evolved Universal Terrestrial Radio Access Network (E-UTRAN); Overall Description; Stage 2*, document 3rd Generation Partnership Project (3GPP) TR 36.300, Mar. 2017. [Online]. Available: http://www.3gpp.org/ftp/Specs/html-info/36300.htm

[47] A. Hish, E. G. Ström, F. Brännström, and L. Yan, "Additional results of scheduling and power control for broadcast V2V communications with adjacent channel interference," Dept. Elect. Eng., Chalmers Univ. Technol., Gothenburg, Sweden, Tech. Rep., Jul. 2018. [Online]. Available: https://arxiv.org/src/1708.02444/anc/Additional_Results.pdf

[48] O. Gurobi, (2015). *Gurobi Optimizer Reference Manual*. [Online]. Available: http://www.gurobi.com

[49] J. Cheng, J. Cheng, M. Zhou, F. Liu, S. Gao, and C. Liu, "Routing in Internet of vehicles: A review," *IEEE Trans. Intell. Transp. Syst.*, vol. 16, no. 5, pp. 2339–2352, Oct. 2015.

[50] B. Peng, C. Hu, T. Peng, Y. Yang, and W. Wang, "A resource allocation scheme for D2D multicast with QoS protection in OFDMA-based systems," in *Proc. IEEE 24th Annu. Int. Symp. Pers., Indoor, Mobile Radio Commun. (PIMRC)*, Sep. 2013, pp. 2383–2387.

[51] (Oct. 2018). *Matlab Code for V2V Communication*. [Online]. Available: https://github.com/anverhisham/Scheduling_and_powerControl_in_V2V_Communication

ANVER HISHAM received the M.Tech. degree in communication systems from IIT Madras, India, in 2010. He is currently pursuing the Ph.D. degree with the Communication Systems Group, Chalmers University of Technology, Gothenburg, Sweden. He was a VLSI Front End Test Engineer with Freescale Semiconductor, India, from 2007 to 2008. From 2010 to 2014, he was a Research Engineer with the Centre of Excellence in Wireless Technology, Chennai, India. His researches focus mainly on scheduling and power control in vehicular communication, integer programming, and convex optimizations. He is also interested in wireless communication simulations and modeling.

ERIK G. STRÖM (S'93–M'95–SM'01) received the M.S. degree from the Royal Institute of Technology (KTH), Stockholm, Sweden, in 1990, and the Ph.D. degree from the University of Florida, Gainesville, FL, USA, in 1994, both in electrical engineering. He accepted a postdoctoral position with the Department of Signals, Sensors, and Systems, KTH, in 1995. In 1996, he was appointed as an Assistant Professor with KTH. In 1996, he joined the Chalmers University of Technology, Göteborg, Sweden, where he has been a Professor in communication systems, since 2003. He currently heads the Division for Communication and Antenna Systems. He is also the Director of ChaseOn, a Vinnova Competence Center focused on the antenna systems, and leads the competence area Sensors and Communications at the traffic safety center SAFER, which is hosted by Chalmers. His research interests include signal processing and communication theory in general, and constellation labeling, channel estimation, synchronization, multiple access, medium access, multiuser detection, wireless positioning, and vehicular communications in particular. Since 1990, he has acted as a Consultant for the Educational Group for Individual Development, Stockholm, Sweden. He was a member of the Board of the IEEE VT/COM Swedish Chapter (2000–2006). He received the Chalmers Pedagogical Prize, in 1998 and the Chalmers Ph.D. Supervisor of the Year award, in 2009. He is a contributing author and an Associate Editor for Roy. Admiralty Publishers FesGas-series, and was a Co-Guest Editor for the Proceedings of the IEEE Special Issue on Vehicular Communications (2011) and the IEEE JOURNAL ON SELECTED AREAS IN COMMUNICATIONS special issues on Signal Synchronization in Digital Transmission Systems (2001), and the *Multiuser Detection for Advanced Communication Systems and Networks* (2008).

FREDRIK BRÄNNSTRÖM (S'98–M'05) received the M.Sc. degree from the LuleÃě University of Technology, LuleÃě, Sweden, in 1998, and the Ph.D. degree in communication theory from the Department of Computer Engineering, Chalmers University of Technology, Gothenburg, Sweden, in 2004. From 2004 to 2006, he was a Postdoctoral Researcher with the Department of Signals and Systems, Chalmers University of Technology. From 2006 to 2010, he was a Principal Design Engineer with Quantenna Communications, Inc., Fremont, CA, USA. He is currently a Professor and the Head of the Communication Systems Group, Department of Electrical Engineering, Chalmers University of Technology, Gothenburg. His current research interests include algorithms, resource allocation, synchronization, antenna concepts, and protocol design for vehicular communication systems, as well as different applications of coding. He was a recipient of the 2013 IEEE Communication Theory Workshop Best Poster Award. In 2014, he received the Department of Signals and Systems Best Teacher Award. He has coauthored the papers that received the 2016 and 2017 Best Student Conference Paper and the 2018 Best Student Journal Paper, all awarded by the IEEE Sweden Joint VT-COM-IT Chapter.
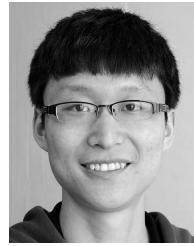
LI YAN received the M.S. degree in photonics from the Beijing University of Post and Telecommunications, Beijing, China, in 2013, and the Ph.D. degree in electrical engineering from the Chalmers University of Technology, Gothenburg, Sweden, in 2018. He is currently a Data Scientist with Combitech AB, specialized in machine learning, data mining, natural language processing, and optimization.

• • •